Antisense oligonucleotide therapy rescues disturbed brain rhythms and sleep in juvenile and adult mouse models of Angelman syndrome

Dongwon Lee[1,2,†], Wu Chen[1,2,†,*], Heet Naresh Kaku[1,2,†], Xinming Zhuo[3,†,‡], Eugene S. Chao[1,2], Armand Soriano[4], Allen Kuncheria[1], Stephanie Flores[1], Joo Hyun Kim[1,2], Frank Rigo[4], Paymaan Jafar-nejad[4], Arthur L. Beaudet[3,§], Matthew S. Caudill[1,5], Mingshan Xue[1,2,3,*]

[1]Department of Neuroscience, Baylor College of Medicine, Houston, Texas 77030, USA

[2]The Cain Foundation Laboratories, Jan and Dan Duncan Neurological Research Institute at Texas Children's Hospital, Houston, Texas 77030, USA

[3]Department of Molecular and Human Genetics, Baylor College of Medicine, Houston, Texas 77030, USA

[4]Ionis Pharmaceuticals, Carlsbad, California 92010, USA

[5]Jan and Dan Duncan Neurological Research Institute at Texas Children's Hospital, Houston, Texas 77030, USA

[†]These authors contributed equally to this work

[‡]Current address: CLIA Laboratory, The Jackson Laboratory for Genomic Medicine, Farmington, Connecticut 06032, USA

[§]Current address: Luna Genetics, Houston, Texas 77054, USA

*For correspondence: mxue@bcm.edu (MX) or wu.chen@bcm.edu (WC)

Abstract (175 words)

UBE3A encodes ubiquitin protein ligase E3A, and in neurons its expression from the paternal allele is repressed by the *UBE3A* antisense transcript (*UBE3A-ATS*). This leaves neurons susceptible to loss-of-function of maternal *UBE3A*. Indeed, Angelman syndrome, a severe neurodevelopmental disorder, is caused by maternal *UBE3A* deficiency. A promising therapeutic approach to treating Angelman syndrome is to reactivate the intact paternal *UBE3A* by suppressing *UBE3A-ATS*. Prior studies show that many neurological phenotypes of maternal *Ube3a* knockout mice can only be rescued by reinstating *Ube3a* expression in early development, indicating a restricted therapeutic window for Angelman syndrome. Here we report that reducing *Ube3a-ATS* by antisense oligonucleotides in juvenile or adult maternal *Ube3a* knockout mice rescues the abnormal electroencephalogram rhythms and sleep disturbance, two prominent clinical features of Angelman syndrome. Importantly, the degree of phenotypic improvement correlates with the increase of Ube3a protein levels. These results indicate that the therapeutic window of genetic therapies for Angelman syndrome is broader than previously thought, and electroencephalogram power spectrum and sleep architecture should be used to evaluate the clinical efficacy of therapies.

Introduction

Angelman syndrome is a rare neurodevelopmental disorder characterized by severe intellectual disability, developmental delay, speech impairment, motor dysfunction, behavioral uniqueness, microcephaly, sleep disturbance, seizures, and abnormal electroencephalogram (EEG) (Williams et al., 2006; Bird, 2014; Buiting et al., 2016). It is caused by loss-of-function of the maternally derived *UBE3A* gene encoding ubiquitin protein ligase E3A (Kishino et al., 1997; Matsuura et

45 al., 1997). *UBE3A* is expressed from both maternal and paternal alleles in non-neuronal cells, but
46 is paternally imprinted in neurons (Albrecht et al., 1997; Rougeulle et al., 1997; Judson et al.,
47 2014). Imprinted expression of *UBE3A* or silence of the paternal allele in neurons is due to a
48 long non-coding RNA, *UBE3A* antisense transcript (*UBE3A-ATS*). *UBE3A-ATS* is expressed
49 from the paternally inherited chromosome and localized in the nucleus to repress *UBE3A in cis*
50 through a transcriptional collision mechanism (Meng et al., 2012; 2013). Thus, loss-of-function
51 of the maternal *UBE3A* leads to the absence of functional UBE3A proteins in neurons.
52
53 Studies in rodent models carrying maternal *Ube3a* loss-of-function mutations have provided
54 insights into Angelman syndrome mechanisms and identified therapeutic strategies. Many
55 disease relevant phenotypes were reported in these Angelman syndrome models (Margolis et al.,
56 2015; Rotaru et al., 2020; Yang, 2020), and some of them are robust and reproducible in
57 different models and laboratories, including motor impairments (e.g., poor performance in
58 rotarod and open-field tests), decreased innate marble burying and nest building behaviors,
59 cortical hyperexcitability (e.g, poly-spikes in EEG), altered EEG power spectrum and sleep
60 pattern, increased susceptibility to seizure induction, and reduced synaptic long-term potentiation
61 (Jiang et al., 1998; Miura et al., 2002; Weeber et al., 2003; Colas et al., 2005; Yashiro et al.,
62 2009; Huang et al., 2013; Meng et al., 2013; Ehlen et al., 2015; Silva-Santos et al., 2015; Judson
63 et al., 2016; Born et al., 2017; Sidorov et al., 2017; Gu et al., 2018; Sonzogni et al., 2018;
64 Copping and Silverman, 2021). Thus, these phenotypes are suitable for evaluating the effects of
65 potential disease-modifying therapies even though some of them may not be clinically relevant.
66 By genetically reinstating *Ube3a* expression from the maternal allele at different developmental
67 ages, rescue experiments in mice show that most of these neurological functions require *Ube3a*

68 during late embryonic and early postnatal development (Silva-Santos et al., 2015; Gu et al.,
69 2018; Rotaru et al., 2018; Sonzogni et al., 2020), suggesting that the therapeutic window for
70 Angelman syndrome may be limited to very young ages.
71
72 Two categories of therapeutic strategies are being actively pursued for Angelman syndrome. One
73 is to target the downstream substrates of UBE3A protein, and the other is to restore *UBE3A* gene
74 expression (Margolis et al., 2015; Yang, 2020; Copping et al., 2021; Elgersma and Sonzogni,
75 2021; Markati et al., 2021). Since the paternal *UBE3A* allele is intact in Angelman syndrome, an
76 attractive approach is to reactivate the silenced paternal *UBE3A* by suppressing *UBE3A-ATS*
77 expression (***Figure 1A***). Indeed, reducing *Ube3a-ATS* levels in mice through genetic
78 manipulations or topoisomerase inhibition results in unsilencing of the paternal *Ube3a* (Huang et
79 al., 2011; Meng et al., 2012; 2013). Antisense oligonucleotides (ASOs) or CRISPR/Cas9
80 targeting the mouse *Ube3a-ATS* can also up-regulate paternal *Ube3a* expression. Administering
81 ASO or adeno-associated virus (AAV) expressing CRISPR/Cas9 to newborn, but not older,
82 maternal *Ube3a* knockout mice rescues a subset of phenotypes (Meng et al., 2015; Wolter et al.,
83 2020; Milazzo et al., 2021; Schmid et al., 2021). Currently, three Phase 1 or Phase 1/2 clinical
84 trials with ASOs targeting *UBE3A-ATS* are underway. Another approach is to directly express an
85 exogenous copy of *UBE3A* by AAV, which also only rescues a subset of phenotypes of maternal
86 *Ube3a* knockout mice when administered postnatally (Daily et al., 2011; Judson et al., 2021).
87 The reversibility of neurological phenotypes at different ages is summarized in ***Supplementary***
88 ***File 1***. These results imply that gene-targeted therapies may have to be administered to late
89 trimester fetuses or newborns to treat Angelman syndrome, as the first postnatal week in mice is
90 generally assumed to be equivalent to the third trimester of human gestation with regard to the

central nervous system development (Zeiss, 2021). This timing of intervention would be difficult because currently Angelman syndrome is diagnosed after at least the first 6 months of life and typically between 1 and 4 years of age (Williams et al., 2006).

However, the reversibility of three robust and clinically relevant phenotypes of Angelman mouse models remains untested, namely cortical hyperexcitability, altered EEG power spectrum, and sleep disturbance. Alterations in EEG power spectrum, particularly an increased in the power of low frequency oscillations (i.e., 1–30 Hz), are well documented in both Angelman syndrome patients and rodent models (Born et al., 2017; Sidorov et al., 2017; Frohlich et al., 2019; Born et al., 2021; Copping and Silverman, 2021). This brain rhythm is a potential biomarker for assessing clinical symptoms because the power in the delta range (2–4 Hz) correlates with symptom severity in Angelman syndrome patients (Hipp et al., 2021; Ostrowski et al., 2021). Similarly, sleep disturbance, another prominent feature of Angelman syndrome (Spruyt et al., 2018), is also recapitulated in the mouse models (Colas et al., 2005; Ehlen et al., 2015; Copping and Silverman, 2021). Hence, to support the ongoing and planned clinical trials, it is crucial to determine to what extent the EEG and sleep deficits are reversible in juvenile and adult Angelman syndrome mouse models because these developmental ages are more clinically relevant than the neonatal period. To address this question, we generated a new mouse *Ube3a* null allele and administered a single dose of ASOs targeting *Ube3a-ATS* to juvenile or adult maternal *Ube3a* knockout mice. We first systematically determined the levels of *Ube3a-ATS* and *Ube3a* transcripts and Ube3a proteins across different brain regions at different timepoints post ASO administration and then evaluated the corresponding EEG and sleep phenotypes.

114 **Results**

115 **Generation of a new *Ube3a* null allele in mice**

116 Our goal was to assess the effect of *Ube3a-ATS*-targeted ASOs in a mouse model of Angelman
117 syndrome. The widely used mouse model is a *Ube3a* knockout allele ($Ube3a^{tm1Alb}$, referred to as
118 $Ube3a^{\Delta e5}$ here to be distinguished from the new allele) that deletes exon 5 (previously named as
119 exon 2), resulting in a premature stop codon in exon 6 (Jiang et al., 1998) (***Figure 1B***). We
120 performed reverse transcription droplet digital PCR (RT-ddPCR) analyses on this *Ube3a*
121 knockout allele with primer sets targeting different exons. Exons 4, 6, and other exons
122 downstream of the deleted exon 5 were still transcribed in the brains of adult heterozygous
123 maternal ($Ube3a^{m\Delta e5/p+}$) and homozygous ($Ube3a^{m\Delta e5/p\Delta e5}$) mutant mice at a level comparable to
124 wild type (WT) mice (***Figure 1C***), possibly due to an escape from nonsense-mediated mRNA
125 decay or an alternative start site. Similarly, *Ube3a* mRNA was only modestly reduced in the
126 livers of $Ube3a^{m\Delta e5/p+}$ and $Ube3a^{m\Delta e5/p\Delta e5}$ mice (***Figure 1C***). Although this knockout allele
127 produces very little full-length functional Ube3a proteins in the brain (Judson et al., 2014; Grier
128 et al., 2015), we sought to create a new *Ube3a* null allele with diminished *Ube3a* mRNA to
129 facilitate the evaluation of ASO efficacy at the transcript level. CRISPR/Cas9 was used to delete
130 the largest *Ube3a* coding exon, exon 6. The resulting allele ($Ube3a^{\Delta e6}$) carries a premature stop
131 codon in exon 7 (***Figure 1B***). RT-ddPCR analyses of adult heterozygous maternal mutant mice
132 ($Ube3a^{m\Delta e6/p+}$) showed that *Ube3a* mRNA was diminished in the brain and reduced in the liver
133 as compared to WT mice (***Figure 1D***). Western blots revealed that Ube3a protein levels in
134 different brain regions of $Ube3a^{m\Delta e6/p+}$ mice were 2–17% of those in WT mice when they were at
135 6 weeks of age or older (see below). Thus, both *Ube3a* mRNA and proteins are diminished in the

136 *Ube3a*$^{m\Delta e6/p+}$ mouse brains. Furthermore, *Ube3a*$^{m\Delta e6/p+}$ mice showed similar rotarod and marble
137 burying phenotypes to previously reported deficits in *Ube3a*$^{m\Delta e5/p+}$ mice (Shi et al., 2022).
138
139 **ASOs targeting *Ube3a-ATS* non-coding RNA up-regulate paternal *Ube3a-YFP* expression**
140 To increase the paternal expression of *Ube3a* in mice, we used two mouse-specific antisense
141 oligonucleotides to downregulate the *Ube3a-ATS* levels. The first one (Ube3a-as) is
142 complementary to a region downstream of the *Snord115* small nuclear RNA cluster, and this
143 sequence was also targeted by the "ASO B" used in a previous study (Meng et al., 2015). The
144 second one (Snord115) is complementary to a sequence that repeats 110 times in the *Snord115*
145 RNAs. To test the effect and visualize the distribution of these two ASOs in the brain, we first
146 used paternal *Ube3a*^{YFP} mice (*Ube3a*$^{m+/pYFP}$) carrying a *yellow fluorescent protein* (*YFP*)-tagged
147 *Ube3a* (Dindot et al., 2008), as downregulating *Ube3a-ATS* is expected to reactivate the paternal
148 *Ube3a-YFP* allele. A non-targeting control ASO, Ube3a-as ASO, or Snord115 ASO was
149 administered to the brains of 3-month-old *Ube3a*$^{m+/pYFP}$ mice by a single unilateral
150 intracerebroventricular (ICV) injection. We visualized Ube3a-YFP expression by
151 immunostaining of YFP 18 days post ASO injection. Maternal *Ube3a*^{YFP} mice (*Ube3a*$^{mYFP/p+}$)
152 exhibited strong Ube3a-YFP in the brain, whereas *Ube3a*$^{m+/pYFP}$ mice receiving the control ASO
153 showed little expression (***Figure 2A,B***). Ube3a-as ASO and Snord115 ASO caused a robust
154 increase in Ube3a-YFP expression throughout the brains of *Ube3a*$^{m+/pYFP}$ mice (***Figure 2A,B***).
155 Although we did not specifically examine different cell types, YFP was observed in several types
156 of GABAergic neurons including cerebellar Purkinje cells, olfactory bulb granule cells, striatal
157 neurons, and interneurons in cortical layer 1, hippocampal stratum oriens, and cerebellar
158 molecular layer (***Figure 2B***). Thus, both Ube3a-as ASO and Snord115 ASO can broadly

159 reactivate the paternal *Ube3a-YFP* allele in neurons including GABAergic neurons throughout
160 the mouse brain *in vivo*.
161
162 **Ube3a-as ASO and Snord115 ASO reactivate paternal *Ube3a* expression in *Ube3a*$^{m\Delta e6/p+}$**
163 **mice**
164 We sought to assess the efficacy of Ube3a-as ASO and Snord115 ASO in our new mouse model
165 of Angelman syndrome across brain regions and over time by systematically determining the
166 Ube3a protein, *Ube3a* mRNA, and *Ube3a-ATS* levels. We first injected male and female
167 *Ube3a*$^{m\Delta e6/p+}$ mice with control, Ube3a-as ASO, or Snord115 ASO and their sex- and age-
168 matched WT littermates with control ASO in parallel at the juvenile age (postnatal days 22.1 ±
169 0.1 (mean ± s.e.m.), range 21–24, n = 56). Brain tissues were harvested from 8 different regions
170 of both hemispheres at 3, 6, or 10 weeks post ASO injections (***Figure 3A***). We used the
171 hemispheres ipsilateral to the ASO injection site for Western blot analyses and the corresponding
172 contralateral hemispheres for reverse transcription quantitative real-time PCR (RT-qPCR)
173 analyses. At 3 weeks post ASO injections, Ube3a-as ASO and Snord115 ASO increased Ube3a
174 protein levels in *Ube3a*$^{m\Delta e6/p+}$ mice to about 28–71% of the WT levels in different brain regions
175 (***Figure 3B,D,E; Figure 3-supplement 1A; Figure 3-supplement 2***). Correlated with this result,
176 *Ube3a-ATS* levels were downregulated by 29–73% (***Figure 4A,B, Figure 4-supplement 1***) and
177 *Ube3a* mRNA levels were increased to about 22–57% of the WT levels (***Figure 4A,B, Figure 4-***
178 ***supplement 1***). The effects of Ube3a-as ASO remained stable for at least 10 weeks. However,
179 the Ub3a protein and *Ub3a* mRNA levels in Snord115 ASO-treated *Ube3a*$^{m\Delta e6/p+}$ mice markedly
180 decreased at 6 weeks post injections and reached to the levels of control ASO-treated
181 *Ube3a*$^{m\Delta e6/p+}$ mice in most brain regions by 10 weeks post injections (***Figure 3B,D,E; Figure 3-***

182 ***supplement 1A; Figure 3-supplement 2; Figure 4A,B; Figure 4-supplement 1***).

183 Correspondingly, by 10 weeks post injections the *Ube3a-ATS* levels in the Snord115 ASO-

184 treated *Ube3a*$^{m\Delta e6/p+}$ mice returned to those in control ASO-treated WT or *Ube3a*$^{m\Delta e6/p+}$ mice

185 (***Figure 4A,B; Figure 4-supplement 1***).

186

187 We further tested the ASOs in adult mice (postnatal days 65.6 ± 0.6 (mean ± s.e.m.), range 56–

188 72, *n* = 55). At 3 weeks post ASO injections, Ube3a-as ASO and Snord115 ASO also

189 significantly reduced *Ube3a-ATS* levels and increased *Ube3a* mRNA and Ube3a protein levels in

190 *Ube3a*$^{m\Delta e6/p+}$ mice (***Figure 3C,D,F; Figure 3-supplement 1B; Figure 3-supplement 2; Figure***

191 ***4A,B; Figure 4-supplement 1***). However, the up-regulation of Ube3a proteins appeared to be

192 slightly less effective in some brain regions (e.g., posterior cortex, thalamus and hypothalamus,

193 and midbrain and hindbrain) than injecting ASOs to juvenile mice (***Figure 3E,F***). Furthermore,

194 the effects of Ube3a-as ASO modestly decreased over the course of 10 weeks post injections,

195 and the reduction in efficacies over time was much more evident for Snord115 ASO (***Figure 3F;***

196 ***Figure 4A,B; Figure 4-supplement 1***).

197

198 Finally, we examined the relationships among *Ube3a-ATS*, *Ube3a* mRNA, and Ube3a protein

199 levels across individual mice and timepoints. *Ube3a-ATS* levels negatively correlated with

200 Ube3a protein and *Ube3a* mRNA levels in *Ube3a*$^{m\Delta e6/p+}$ mice (***Figure 4C; Figure 4-supplement***

201 ***2A***), and Ube3a protein levels positively correlated with *Ube3a* mRNA levels (***Figure 4-***

202 ***supplement 2B***). Since the protein and transcript levels were measured at the same post ASO

203 injection timepoints from the ipsilateral and contralateral hemispheres, respectively, these

204 correlations indicate a broad distribution of ASOs in the mouse brains and a spatiotemporally

205 comparable pattern between the changes in transcripts and proteins. Taken together, our results
206 demonstrate that a single unilateral ICV injection of ASO targeting *Ube3a-ATS* in *Ube3a*$^{m\Delta e6/p+}$
207 mice leads to a long-lasting down-regulation of this transcript and reactivation of the paternal
208 *Ube3a* allele throughout the brains, and the up-regulation of Ube3a proteins by Ube3a-as ASO
209 can last at least 10 weeks.
210
211 **Reactivation of paternal *Ube3a* expression alleviates abnormal EEG rhythmic activity in**
212 ***Ube3a*$^{m\Delta e6/p+}$ mice**
213 Maternal *Ube3a* deficiency in mice causes altered brain rhythms, sleep disturbance, and
214 epileptiform activity (e.g., cortical poly-spikes), all of which can be examined by chronic video-
215 EEG and electromyogram (EMG) recordings. Thus, to determine if up-regulation of paternal
216 *Ube3a* expression can reverse these phenotypes in *Ube3a*$^{m\Delta e6/p+}$ mice, we injected male and
217 female *Ube3a*$^{m\Delta e6/p+}$ mice with control, Ube3a-as, or Snord115 ASO and their sex- and age-
218 matched WT littermates with control ASO in parallel at the juvenile (postnatal days 21.5 ± 0.1
219 (mean ± s.e.m.), range 21–24, n = 35) or adult (postnatal days 62.5 ± 0.6 (mean ± s.e.m.), range
220 56–66, n = 28) age. Intracranial EEG from the frontal, somatosensory, and visual cortices and
221 EMG from the neck muscles of each mouse were recorded at 3, 6, and 10 weeks post ASO
222 injections (***Figure 3A, Figure 5A***). To avoid bias, we evenly sampled 6 out of 24 hours of the
223 EEG/EMG data for power spectrum and poly-spikes analyses and used 24 hours of data for sleep
224 scoring (see **Materials and Methods**).
225
226 We first removed artifacts and then computed the absolute power spectral densities (PSDs) of
227 EEG signals including all brain states (***Figure 5-supplement 1***). To control for the variations

228 caused by different impedances across electrodes and mice, we normalized PSDs by the total
229 power within 1–100 Hz to obtain the relative PSDs. The relative PSDs from the frontal cortex of
230 control ASO-treated *Ube3a*$^{m\Delta e6/p+}$ mice were higher at 4–25 Hz and lower at 40–80 Hz than
231 those of control ASO-treated WT mice (***Figure 5B,E***). Thus, we further computed the relative
232 power in the frequency bands of delta (δ, 1–4 Hz), theta (θ, 4–8 Hz), alpha (α, 8–13 Hz), low
233 beta (β1, 13–18 Hz), high beta (β2, 18–25 Hz), low gamma (γ1, 25–50 Hz), and high gamma (γ2,
234 50–100 Hz) (***Figure 5C,F***). To capture the concurrent changes in both low and high frequency
235 ranges, we calculated the ratio of the total power in the alpha, low beta, and high beta bands over
236 the power in high gamma band (i.e., (α+β1+β2)/γ2). This ratio represents the relative
237 distribution of power between the low and high frequency bands and importantly, is independent
238 from the use of PSD or relative PSD. We discovered that the power ratio (α+β1+β2)/γ2 was
239 higher in control ASO-treated *Ube3a*$^{m\Delta e6/p+}$ mice than control ASO-treated WT mice across all
240 time points (***Figure 5D,G***). Similar phenotypes were also observed in the somatosensory cortex
241 (***Figure 5-supplement 2***), but the EEG rhythmic activity in the visual cortex was not
242 significantly altered in control ASO-treated *Ube3a*$^{m\Delta e6/p+}$ mice (***Figure 5-supplement 3***). These
243 results indicate that maternal *Ube3a* deficiency alters EEG rhythms in the frontal and
244 somatosensory cortices, and the power ratio (α+β1+β2)/γ2 can be a robust measure of the effects
245 of Ube3a-as and Snord115 ASOs.
246
247 Treating *Ube3a*$^{m\Delta e6/p+}$ mice with Ube3a-as ASO at the juvenile age caused a decrease of the
248 power in the alpha, low beta, and high beta bands and an increase of the power in the high
249 gamma band, particularly at 3 and 6 weeks post ASO injections (***Figure 5C***), which led to the
250 normalization of the ratio (α+β1+β2)/γ2 in the frontal and somatosensory cortices, as the ratios

251 in Ube3a-as ASO-treated *Ube3a*$^{m\Delta e6/p+}$ mice were indistinguishable from those in control ASO-
252 treated WT mice (***Figure 5D; Figure 5-supplement 2C***). In contrast, Snord115 ASO only
253 showed such effects in the frontal cortex at 3 weeks post ASO injections, and the effects waned
254 at later timepoints (***Figure 5C,D***). This difference between Ube3a-as ASO and Snord115 ASO
255 generally correlates with their difference in up-regulating Ube3a proteins (see below). When
256 *Ube3a*$^{m\Delta e6/p+}$ mice were treated with ASOs at the adult age, Ube3a-as ASO and Snord115 ASO
257 were also able to reduce the power in the low frequency bands and increased the power in the
258 high gamma band in the frontal cortex (***Figure 5E,F***), thereby reducing the ratio $(\alpha+\beta1+\beta2)/\gamma2$
259 (***Figure 5G***). These effects also waned over time, consistent with the change of Ube3a protein
260 levels (***Figure 3F***). Altogether, these results show that upon reactivation of the paternal *Ube3a*
261 by *Ube3a-ATS* targeted ASOs in juvenile or adult *Ube3a*$^{m\Delta e6/p+}$ mice, the abnormal EEG
262 rhythmic activity in *Ube3a*$^{m\Delta e6/p+}$ mice can be reversed in a Ube3a protein level-dependent
263 manner.
264
265 **Reactivation of paternal *Ube3a* expression restores normal sleep pattern in *Ube3a*$^{m\Delta e6/p+}$**
266 **mice**
267 To study the sleep architecture, we used the EEG and EMG signals and a convolutional neural
268 network-based algorithm SPINDLE (Miladinović et al., 2019) to classify the brain states into
269 rapid eye movement (REM) sleep, non-rapid eye movement (NREM) sleep, and wake
270 throughout 24 hours (***Figure 6-supplement 1A***). The difference in the EEG PSDs did not affect
271 the accuracy of SPINDLE (***Figure 6-supplement 1B,C***). Overall, mice spent more time in REM
272 and NREM sleep and less time in wake during the light phase than the dark phase (***Figure 6***).
273 The time in wake was similar between control ASO-treated WT and *Ube3a*$^{m\Delta e6/p+}$ mice across

274 ages (***Figure 6C,F***). Control ASO-treated *Ube3a*$^{m\Delta e6/p+}$ mice spent significantly less time in
275 REM sleep than control ASO-treated WT mice in the light phase, but this phenotype was more
276 variable in adult mice (***Figure 6A,D***). Correspondingly, control ASO-treated *Ube3a*$^{m\Delta e6/p+}$ mice
277 spent slightly more time in NREM sleep than control ASO-treated WT mice because REM sleep
278 is a small fraction of the total sleep (***Figure 6B,E***). Thus, the sleep disturbance in *Ube3a*$^{m\Delta e6/p+}$
279 mice manifests as a selective reduction in REM sleep, which recapitulates the observation in
280 Angelman patients (Miano et al., 2004; 2005).
281
282 Administering Ube3a-as ASO or Snord115 ASO to juvenile *Ube3a*$^{m\Delta e6/p+}$ mice increased their
283 time in REM sleep at 3 and 6 weeks post ASO injections, thereby normalizing their sleep pattern,
284 as their time in REM sleep was indistinguishable from that in control ASO-treated WT mice
285 (***Figure 6A***). This effect was reduced at 10 weeks post ASO injections (***Figure 6A***). When
286 *Ube3a*$^{m\Delta e6/p+}$ mice were treated with ASOs at the adult age, Ube3a-as ASO and Snord115 ASO
287 were less effective in restoring REM sleep (***Figure 6D***). Overall, these results indicate that the
288 sleep disturbance in *Ube3a*$^{m\Delta e6/p+}$ mice can be rescued by reactivation of the paternal *Ube3a* in
289 juvenile mice.
290
291 **Partial restoration of Ube3a protein levels does not suppress cortical hyperexcitability in**
292 ***Ube3a*$^{m\Delta e6/p+}$ mice**
293 Most Angelman syndrome patients develop epileptic seizures within the first three year of age
294 (Williams et al., 2006; Bird, 2014). Although maternal *Ube3a* knockout mice or rats do not
295 develop spontaneous seizures, they exhibit cortical hyperexcitability and epileptiform activity,
296 manifesting as numerous poly-spikes (Mandel-Brehm et al., 2015; Born et al., 2017; 2021).

297 Indeed, control ASO-treated *Ube3a*$^{m\Delta e6/p+}$ mice showed significantly more poly-spikes in the
298 frontal and somatosensory cortices than control ASO-treated WT mice (***Figure 7A–C; Figure 7-***
299 ***supplement 1A,C***). Interestingly, the visual cortices of control ASO-treated *Ube3a*$^{m\Delta e6/p+}$ mice
300 did not exhibit this epileptiform activity (***Figure 7-supplement 1B,D***). Ube3a-as ASO or
301 Snord115 ASO treatment of juvenile *Ube3a*$^{m\Delta e6/p+}$ mice did not significantly reduce poly-spikes
302 as compared to control ASO, although Snord115 ASO-treated *Ube3a*$^{m\Delta e6/p+}$ mice showed a 50%
303 reduction in the number of poly-spikes (***Figure 7B; Figure 7-supplement 1A***). Similarly,
304 treating adult *Ube3a*$^{m\Delta e6/p+}$ mice with Ube3a-as ASO or Snord115 ASO did not cause a
305 significant decrease of poly-spikes at any time point (***Figure 7C; Figure 7-supplement 1C***).
306 Thus, these results indicate that under our experimental conditions where Ube3a protein levels
307 are partially restored in juvenile or adult *Ube3a*$^{m\Delta e6/p+}$ mice, their cortical hyperexcitability
308 phenotype cannot be reversed.
309
310 **Modulation of EEG rhythms and REM sleep by ASOs tracks the Ube3a protein levels in**
311 ***Ube3a*$^{m\Delta e6/p+}$ mice**
312 Our results above show that Ube3a-as ASO and Snord115 ASO up-regulate Ube3a proteins
313 (***Figure 3; Figure 3-supplement 2***) and modulate EEG rhythms (***Figure 5***) and REM sleep
314 (***Figure 6***) to different extents in *Ube3a*$^{m\Delta e6/p+}$ mice depending on the age of ASO injection and
315 post-injection time. To understand how well the modulation of EEG rhythms and REM sleep by
316 the ASOs reflects the Ube3a protein levels, we determined the relationships between Ube3a
317 protein levels and EEG relative power in different frequency bands, power ratio $(\alpha+\beta1+\beta2)/\gamma2$,
318 or time in REM sleep. We first averaged the Ube3a protein levels across different brain regions
319 to estimate the overall Ube3a protein levels in each mouse from the Western blot experiments

320 (***Figure 3; Figure 3-supplement 2***) and then obtained the mean Ube3a protein levels at each of
321 the 3-, 6-, and 10-week timepoints post ASO injections. Since the Ube3a protein levels in
322 *Ube3a*$^{m\Delta e6/p+}$ mice were expressed a fraction of the WT levels, for the corresponding EEG
323 relative power in different frequency bands, power ratio (α+β1+β2)/γ2, and time in REM sleep,
324 we also normalized the data by the means of those in the corresponding control ASO-treated WT
325 mice. For both ASO injections into juvenile and adult mice, the relative power in the theta (θ, 4–
326 8 Hz), alpha (α, 8–13 Hz), low beta (β1, 13–18 Hz), and high beta (β2, 18–25 Hz) band
327 negatively correlated with the Ube3a protein levels, whereas the relative power in the low
328 gamma (γ1, 25–50 Hz) and high gamma (γ2, 50–100 Hz) band positively correlated with the
329 Ube3a protein levels. Therefore, the power ratio (α+β1+β2)/γ2 also negatively correlated with
330 the Ube3a protein levels (***Figure 8A***). However, the relative power in the delta (δ, 1–4 Hz) band
331 did not correlate with the Ube3a protein levels (***Figure 8A***). Finally, the time in REM sleep
332 during the light phase positively correlated with the Ube3a protein levels too (***Figure 8B***). In the
333 dark phase, the positive correlation between the time in REM sleep and the Ube3a protein levels
334 existed only for the ASO injection into the juvenile mice (***Figure 8B***). Hence, these results
335 indicate that the relative power of EEG rhythms and time in REM sleep dynamically follow the
336 Ube3a protein levels in *Ube3a*$^{m\Delta e6/p+}$ mice that are regulated by the ASOs.
337

338 **Discussion**

339 Genetic approaches to restoring *UBE3A* expression holds great promise for treating Angelman
340 syndrome because they tackle the disease root cause. Three active clinical trials of *UBE3A-ATS*-
341 targeted ASOs have generated a great deal of excitement and expectation in the community.
342 Meanwhile, an increasing number of studies in mouse models of Angelman syndrome

343 demonstrate that *Ube3a* must be reinstated in late embryonic and early postnatal development to
344 correct most neurological phenotypes. Among the previously tested phenotypes, only a small
345 subset (i.e., synaptic transmission, plasticity, and spatial memory) can be improved upon
346 increasing Ube3a at the age of 6 weeks or older, and slightly a few more (i.e., rotarod
347 performance and susceptibility to seizure induction) when increasing Ube3a at postnatal day 21
348 (***Supplementary File 1***). Despite limited prior successes in rescuing juvenile and adult maternal
349 *Ube3a* deficiency mice, we chose these two ages to examine the effects of ASO therapy on
350 cortical hyperexcitability, altered EEG power spectrum, and sleep disturbance because these ages
351 are more translationally relevant than the neonatal period. Our study reveals that a single ICV
352 injection of *Ube3a-ATS*-targeted ASOs to *Ube3a*$^{m\Delta e6/p+}$ mice, a new rodent model of Angelman
353 syndrome, restores the EEG power spectrum and sleep pattern for at least 6 weeks, particularly
354 upon treatment at the juvenile age. Therefore, our results significantly expand the range of
355 phenotypes that can be reversed by restoring *Ube3a* expression in juvenile and adult mice.
356 Interestingly, we were not able to reduce the frequency of poly-spikes in *Ube3a*$^{m\Delta e6/p+}$ mice at
357 either age (***Figure 7***). It is possible that suppression of poly-spikes requires up-regulation of
358 Ube3a starting at a younger age or reaching to a higher level than what we have achieved, both
359 of which should be tested in future studies. Nevertheless, this result indicates that poly-spikes are
360 independent from the EEG power spectrum and sleep pattern deficits, and probably involve a
361 different mechanism.
362
363 A critical finding of our study is that the improvement in the EEG power spectrum and sleep
364 pattern tracks the increase in Ube3a protein levels across different ASOs, injection ages, and
365 timepoints post injection (***Figure 8***). This suggests that following a bolus injection of ASOs,

366 both phenotypes are acutely modulated by the Ube3a levels that decrease over time due to ASO
367 clearance. Future studies should determine if repeated administration of ASOs can generate a
368 long-lasting improvement of the phenotypes beyond the period when Ube3a levels are
369 sufficiently up-regulated, as the outcome can help inform the ASO treatment schedule in clinical
370 trials. The ASO treatment in adult mice is less effective than juvenile mice, possibly due to two
371 reasons. First, the reversibility of these two phenotypes may decrease over age, just like other
372 neurological deficits (***Supplementary File 1***). Second, the ASO treatment in adult mice causes a
373 smaller increase of Ube3a protein than juvenile mice (***Figure 3***). Given the strong correlation
374 between Ube3a levels and phenotypic improvement, we speculate that the latter is more likely
375 the reason and a higher dose of ASO or an ASO with a higher efficacy in down-regulating
376 *Ube3a-ATS* should further increase Ube3a protein and improve these two phenotypes in adult
377 mice.
378
379 Previous EEG studies of *Ube3a*$^{m\Delta e5/p+}$ mice emphasized an increase of absolute power or PSD in
380 the delta frequency band as compared to WT mice, but the results varied among studies (Ehlen et
381 al., 2015; Born et al., 2017; Sidorov et al., 2017; Copping and Silverman, 2021). One study
382 recorded local field potential in layer 4 of the primary visual cortex from awake mice that were
383 head-fixed and viewing a static gray screen. The absolute delta (2–4 Hz) power of local field
384 potential was increased when *Ube3a*$^{m\Delta e5/p+}$ mice were on a 129 strain background, but not on a
385 C57BL/6 background. Interestingly, a reduction of the relative power in the gamma band (30–50
386 Hz) was observed in both strains (Sidorov et al., 2017). In contrast, two other studies reported an
387 increase in delta (0–4 or 0.5–4 Hz) power of chronic EEG recorded from the cortical surface of
388 freely moving *Ube3a*$^{m\Delta e5/p+}$ mice on a C57BL/6 background (Born et al., 2017; Copping and

389 Silverman, 2021), but not on a 129 strain background (Born et al., 2017). Finally, it was reported
390 that the relative delta power of cortical surface EEG was reduced in *Ube3a*$^{m\Delta e5/p+}$ mice on the
391 C57BL/6J background during NREM sleep in the night, but not in the day (Ehlen et al., 2015).
392 Our absolute PSD results from the new *Ube3a*$^{m\Delta e6/p+}$ mice are qualitatively similar to the
393 previous results (***Figure 5-supplement 1***), but relative PSD analysis reveals an increase of
394 relative power in the theta, alpha, or beta frequency bands and a decrease in the low or high
395 gamma frequency bands. These differences could be due to different mutations, genetic
396 backgrounds, mouse ages, experimental conditions, or different brain states included in the
397 analyses. Nevertheless, we observed a robust and consistent increase in the power ratio
398 $(\alpha+\beta1+\beta2)/\gamma2$ across timepoints (***Figure 5***). In fact, inspection of previous results suggests a
399 common pattern that EEG power is relatively higher in maternal *Ube3a* deficiency mice than
400 WT mice in the lower frequency bands (i.e., beta or lower) and relatively lower in the gamma
401 bands, although the results were not always statistically significant (Born et al., 2017; Sidorov et
402 al., 2017; Copping and Silverman, 2021). Similarly, the EEG power spectrum of Angelman
403 syndrome patients also shows such a pattern (Sidorov et al., 2017). Thus, we propose that a
404 power ratio between the low and high frequency bands would be a more robust measure of the
405 EEG power spectrum phenotype in Angelman syndrome and its mouse models.
406
407 The EEG power spectrum and sleep phenotypes of maternal *Ube3a* knockout mice directly
408 correlate with those in Angelman syndrome patients, but about 70% of Angelman syndrome
409 patients have a larger deletion on chromosome 15 at 15q11-q13 that encompasses *UBE3A* and
410 other genes (Bird, 2014; Buiting et al., 2016). Thus, future studies are necessary to determine the
411 contribution of other genes to the neurological phenotypes including disturbed EEG power

412 spectrum and sleep and to what extent reactivating paternal *Ube3a* can rescue these phenotypes
413 in a deletion mouse model. Nevertheless, our study has several translational implications for the
414 ASO and other clinical trials of Angelman syndrome. First, even though it is unclear how the
415 mouse developmental stages in which the neurological phenotypes can be reversed are related to
416 the treatment window for Angelman syndrome, our results suggest is that Angelman syndrome
417 patients at different ages may all benefit from the ASO treatment of these two core disease
418 symptoms. Second, the robust correlation between EEG power spectrum and Ube3a levels
419 supports the notion that EEG power spectrum can serve as a quantitative biomarker in clinical
420 trials (Sidorov et al., 2017; Frohlich et al., 2019; Hipp et al., 2021; Ostrowski et al., 2021). Third,
421 the EEG power of Angelman syndrome patients correlates with their symptom severity,
422 particularly the cognitive function (Hipp et al., 2021; Ostrowski et al., 2021). Since the synaptic
423 plasticity and spatial memory phenotypes of maternal *Ube3a* knockout mice are still reversible in
424 adulthood (Daily et al., 2011; Meng et al., 2015; Silva-Santos et al., 2015; Milazzo et al., 2021),
425 it is reasonable to speculate that ASO treatment may also improve the cognitive function of
426 Angelman syndrome patients. Finally, clinicians and caregivers consider sleep disturbance as
427 one of the most challenging symptoms and important focuses for new treatment (Willgoss et al.,
428 2021). Thus, if ASO therapy can reduce sleep disturbance, then it will improve quality of life for
429 both Angelman syndrome patients and caregivers.
430

431 **Materials and Methods**

432 **Mice**

433 The new *Ube3a* null allele was generated by CRISPR/Cas9-mediated deletion of exon 6. Wild
434 type *Cas9* mRNA (100 ng/µl) and two sgRNAs (10 ng/µl each) targeting the genomic sequences

435 of *Ube3a* intron 5 (5′-TTACATACCAGTACATGTCTTGG-3′) and intron 6 (5′-
436 TGCTTTCTACCAACTGAGACAGG-3′) were microinjected into C57BL/6J WT zygotes.
437 Founder mice carrying the exon 6 deletion (*Ube3a*$^{\Delta e6}$) were identified by PCR using a pair of
438 primers (5′-TTGAGAACAATGCAAAGGAAAATGA-3′ and 5′-
439 GAGCAAACTGCTGTAGACCC-3′) for the WT allele (747 bp) and a pair of primers (5′-
440 TTGAGAACAATGCAAAGGAAAATGA-3′ and 5′-TGAGGCTGGCTTTCAAGATTCA-3′)
441 for the *Δe6* (314 bp) allele. Founder mice were then backcrossed to C57BL/6J WT mice to
442 generate N1 mice. N1 mice carrying the *Δe6* allele were identified using the same PCR above.
443 Sequencing of the identified N1 mice confirmed that the sequence chr7:59,275,513–59,277,423
444 were deleted. *Ube3a*$^{\Delta e6}$ mice were backcrossed to C57BL/6J WT mice for at least 5 generations
445 prior to experiments. Heterozygous female mice carrying the mutation on their paternal
446 chromosome (*Ube3a*$^{m+/p\Delta e6}$) were crossed with C57BL/6J WT mice to generate WT and maternal
447 knockout of *Ube3a* mice (*Ube3a*$^{m\Delta e6/p+}$).
448
449 *Ube3a*^{YFP} mice (JAX #017765) were described previously (Dindot et al., 2008) and carry a
450 *Ube3a* knockin allele with a yellow fluorescent protein (YFP) fused to the C terminus of Ube3a.
451 Heterozygous male or female mice carrying *Ube3a-YFP* on their paternal chromosome
452 (*Ube3a*$^{m+/pYFP}$) were crossed with wildtype (WT) C57BL/6J mice (JAX #000664) to obtain
453 heterozygous paternal or maternal *Ube3a*^{YFP} mice (*Ube3a*$^{m+/pYFP}$ or *Ube3a*$^{mYFP/p+}$), respectively.
454 Both *Ube3a*^{YFP} and *Ube3a*$^{\Delta e6}$ alleles were maintained on the C57BL/6J background. Mice were
455 housed in an Association for Assessment and Accreditation of Laboratory Animal Care
456 International-certified animal facility on a 14-hour/10-hour light/dark cycle. All procedures to

457 maintain and use mice were approved by the Institutional Animal Care and Use Committee at
458 Baylor College of Medicine.
459
460 **Reverse transcription droplet digital PCR (ddPCR)**
461 Mice were anesthetized and decapitated. Brain and liver tissues were extracted and homogenized
462 with Trizol™ (ThermoFisher, catalog #15596026), followed by RNase-free DNase treatment
463 (Qiagen, catalog #79254). RNAs were purified with RNeasy Plus Mini Kit (Qiagen, catalog
464 #74136) and reverse transcribed to cDNA by High-Capacity cDNA Reverse Transcription Kit
465 (ThermoFisher, catalog #4368814). The cDNA concentration was determined by a Nanodrop
466 (ThermoFisher). Droplet digital PCR (ddPCR) was prepared by mixing the following reagents in
467 a total volume of 20 µl: 2x QX200 ddPCR EvaGreen supermix (Biorad, catalog #1864036, 10
468 µl), forward and reverse primers (10 µM, 0.4 µl each), cDNA template (10–100 ng, 1 µl), and
469 nuclease-free H_2O (8.2 µl). The droplets for ddPCR were generated by a Biorad Automated
470 Droplet Generator (Biorad, catalog #1864101), followed by PCR reaction using a Thermal
471 Cycler C1000 (Biorad). The plate containing the droplets was read by a QX200 Droplet reader
472 (Biorad, catalog #1864001). The primers for detecting different fragments of the *Ube3a*
473 transcripts are provided in ***Supplementary File 2***. The expression levels of *Ube3a* transcripts
474 were normalized by the *Gapdh* levels.
475
476 **Antisense oligonucleotides (ASOs)**
477 Synthesis and purification of all chemically modified oligonucleotides were performed as
478 previously described (Swayze et al., 2007). The 2′-*O*-methoxyethylribose (MOE) gapmer ASOs
479 are 20 nucleotides in length, wherein the central gap segment comprising ten 2′-

480 deoxynucleotides is flanked on the 5′ and 3′ wings by five 2′-MOE modified nucleotides. All
481 internucleoside linkages are phosphorothioate linkages, except the ones shown as "o" in the
482 sequences which are phosphodiester. The sequences of the ASOs are as follows: control ASO,
483 5′-CCToAoToAoGGACTATCCAoGoGAA-3′; Ube3a-as ASO, 5′-
484 CCoAoGoCoCTTGTTGGATAoToCAT-3′; and Snord115 ASO, 5′-
485 TToGoToAoAGCATCAAAGToAoTGA-3′. Lyophilized ASOs were formulated in phosphate
486 buffered saline (PBS) without Ca^{2+} and Mg^{2+} (Gibco, catalog # 14190). ASOs were dissolved in
487 PBS to obtain 50 mg/ml concentrations.
488
489 **Intracerebroventricular (ICV) injection of ASOs**
490 Mice were anesthetized with isoflurane (1.5–2.5 %) in oxygen (1 l/min). The body temperature
491 was monitored and maintained at 37°C using a temperature controller (ATC-2000, World
492 Precision Instruments). An incision was made along the midline to expose the skull after the
493 head was fixed in a stereotaxic apparatus. Approximately 0.25 mm-diameter craniotomies were
494 performed with a round bur (0.25 mm diameter) and a high-speed rotary micromotor (EXL-M40,
495 Osada) at the injection site (see below). A bevelled 50 µm-diameter glass pipette was used to
496 inject ASOs into the right lateral ventricle according to one of the following sets of coordinates
497 that were normalized by the distance between Bregma and Lambda (DBL). 1) Anterior/posterior
498 (AP): 0.055 of DBL, medial/lateral (ML): 0.238 of DBL, dorsal/ventral (DV): -0.499 of DBL; 2)
499 AP: 0.055 of DBL, ML: 0.238 of DBL, DV: -0.594 of DBL; 3) AP: 0.071 of DBL, ML: 0.238 of
500 DBL, DV, -0.713 of DBL. The results were similar among these three sets of coordinates and
501 were grouped together. ASO solution was injected at a rate of 407 nl/s using an UltraMicroPump
502 III and a Micro4 controller (World Precision Instruments). A total of 10 µl ASO solution (50

503 mg/ml) was administered for a total dosage of 500 µg/mouse except 6 mice that were injected
504 with 5 µl ASO solution for a total dosage of 250 µg/mouse at the age of 3 weeks and used in the
505 Western blot experiments. The results from these 6 mice were similar to other mice (***Figure 3-***
506 ***supplement 3***) and grouped together. After injection, the pipette was held in place for 10 min
507 before withdrawal. The skin was sutured, and mice were allowed to recover from anesthesia in a
508 cage placed on a heating pad. When the recovery takes longer than 1 hour, the duration on the
509 heating pad should not exceed 1 hour, as longer exposure of mice on the heating pad
510 significantly reduces post-surgery survival rates (less than 1 hour: 1 out of 102 injected mice
511 died, more than 1 hour: 31 out of 106 injected mice died, $P < 0.0001$).
512
513 **Immunohistochemistry and fluorescent microscopy**
514 Mice were anesthetized and transcardially perfused with PBS (pH 7.4) followed by 4%
515 paraformaldehyde in PBS (pH 7.4). Brains were then post-fixed for overnight in 4%
516 paraformaldehyde at 4℃ and sectioned into 40 µm sagittal slices using a vibratome (VT1000S,
517 Leica). Brain sections were incubated in blocking solution (0.2% Triton X-100 in PBS with 5%
518 normal goat serum) for 1 hr at 4°C and then with a primary antibody anti-GFP (Invitrogen,
519 catalog # G10362, lot # 1965886, 1:2000 dilution) that recognizes YFP for overnight at 4°C.
520 Sections were washed with 0.2% Triton X-100 in PBS and then incubated with a goat anti-rabbit
521 secondary antibody conjugated with Alexa Flour 647 (Invitrogen, catalog # A21245, lot #
522 1623067, 1:1000 dilution) in blocking solution for 3 hr at room temperature. After antibody
523 staining, sections were incubated with NeuroTrace 435/455 blue fluorescent Nissl stain
524 (Invitrogen, catalog #N21479, 1:200 dilution) in 0.2% Triton X-100 in PBS at room temperature
525 for 1 hr to label neurons. Sections were washed with 0.2% Triton X-100 in PBS and mounted in

526 ProLong Diamond Antifade Mountant (Invitrogen, catalog # P36961). High resolution
527 (1024×1024) single plane images of the brain sections were acquired on a TCS SP8X Confocal
528 Microscope (Leica) using a 20 × oil objective (HC PL APO CS2 20×, NA = 0.75). Mosaic
529 images were stitched together using LAS X software v3.3.0.16799 (Leica) and visualized and
530 exported by ImageJ 1.53c (NIH).
531
532 **Western blot and reverse transcription quantitative real-time PCR (RT-qPCR)**
533 Mice were anesthetized and decapitated. The brains were extracted, and different regions were
534 dissected from both hemispheres. The brain tissues from the right hemisphere were used for
535 Western blots and the left hemisphere for RT-qPCR. Tissues were frozen at -80°C until analysis.
536
537 For Western blots, the brain tissues were homogenized in RIPA buffer containing 50 mM Tris-
538 HCl (pH 8.0), 150 mM NaCl, 1% Triton X-100, 0.5% Na-deoxycholate, 0.1% SDS, 1 mM
539 EDTA, 5% glycerol, and 1 cOmplete™ Protease Inhibitor tablet (Roche, # SKU 11836170001).
540 After homogenization, tissue debris was removed by centrifugation and protein concentrations
541 were determined by Pierce BCA Protein Assay Kit (ThermoFisher Scientific, catalog # 23225).
542 10 µg of proteins per sample were resolved by SDS-PAGE and transferred onto nitrocellulose
543 membranes. Ube3a was detected by a mouse anti-E6AP (Sigma, catalog # E8655, lot #
544 118M4792V, 1:1000 dilution) and a mouse anti-Gapdh (Proteintech, catalog # 60004-1-Ig, lot #
545 10004129, 1:10,000 dilution) antibodies. Primary antibodies were detected by a goat anti-mouse
546 antibody conjugated with IRDye 800CW (LI-COR Bioscience, catalog # 925-32210, lot #
547 C90130-03, 1:20,000 dilution). Proteins were visualized and quantified using an Odyssey CLx
548 Imager and Image Studio Lite version 5.2 (LI-COR Biosciences). Both long and short Ube3a

549 isoforms were included together in the quantification. Ube3a levels were first normalized by the
550 Gapdh levels and then by the average Ube3a levels of all WT mice from the same blot.
551
552 For RT-qPCR, the brain tissues were homogenized in RLT buffer (Qiagen, catalog # 79216)
553 containing 1% (v/v) β-mercaptoethanol. Homogenization was performed for 20 s at 6000 rpm
554 using a FastPrep Automated Homogenizer (MP Biomedicals). Total RNA was then purified
555 using the RNeasy 96 Kit (Qiagen, catalog # 74182) that included an in-column DNA digestion
556 with 50 U of DNase I (Invitrogen, catalog # 18047019). RT-qPCR was performed in triplicate
557 with the EXPRESSS One-Step SuperScript qRT-PCR kit (ThermoFisher Scientific, catalog #
558 11781200). Gene-specific primers and probes are provided in ***Supplementary File 2***. The
559 expression levels of *Ube3a* or *Ube3a-ATS* were normalized by the *Gapdh* levels and then by the
560 average *Ube3a* or *Ube3a-ATS* levels of all WT mice from the same experiment, respectively.
561
562 **Video-electroencephalogram(EEG) and electromyogram (EMG) recordings**
563 Video-EEG/EMG recordings were performed as previously described (Chen et al., 2020).
564 Briefly, one week after ASO injection, mice were anesthetized with 2.5% isoflurane in oxygen,
565 and craniotomies were performed as described above for ICV injection. Perfluoroalkoxy polymer
566 (PFA)-coated silver wire electrodes (A-M Systems, catalog # 786000, 127 mm bare diameter,
567 177.8 mm coated diameter) were used for grounding at the right frontal cortex, referencing at the
568 cerebellum, and recording at the left frontal cortex (AP: 0.475 of DBL, ML: -0.071 of DBL, DV:
569 -1.5 mm), left somatosensory cortex (AP: -0.190 of DBL, ML: -0.428 of DBL, DV: -1.5 mm),
570 and right visual cortex (AP: -0.808 of DBL, ML: 0.594 of DBL, DV: -1.5 mm). An EMG
571 recording and an EMG reference electrode were inserted into the neck muscles. All electrodes

572 were soldered to an adaptor prior to the surgery. The electrodes and adaptor were secured on the
573 skull by dental acrylic. The skin was sutured and attached to the dried dental acrylic. Mice were
574 singly housed to recover for at least one week after the surgeries. Before recording, mice were
575 individually habituated in the recording chambers (10-inch diameter of Plexiglas cylinder) for 24
576 hours. EEG/EMG signals (5000-Hz sampling rate with a 0.5-Hz high-pass filter) and videos (30
577 frames per second) were recorded synchronously for more than 48 continuous hours using a 4-
578 channel EEG/EMG tethered system and Sirenia 1.8.2 software (Pinnacle Technology).
579
580 **EEG poly-spikes and power spectrum analyses**
581 Poly-spikes and power spectral density (PSD) were analyzed from the same 6 hours of each
582 recording (12 AM–1 AM, 4 AM–5 AM, 8 AM–9 AM, 12 PM–1 PM, 4 PM–5 PM, and 8 PM–9
583 PM on the second day). EEG/EMG traces were visualized in Sirenia Seizure 1.8.2 software
584 (Pinnacle Technology) to identify episodes of poly-spikes and artifacts. An episode of poly-
585 spikes is defined as a cluster of three or more spikes on any of the EEG channels. PSD analyses
586 of EEG data were performed using custom scripts in Python. Prior to PSD calculation, data were
587 detrended by subtracting the mean of the data. The data segments containing artifacts on any of
588 the EEG channels were first excluded, and then an 8th order Butterworth filter was applied to
589 each channel to bi-directionally notch filter around 60 Hz (± 2 Hz bandwidth) to remove power-
590 line noise. The PSDs were then estimated for each channel using a Welch's periodogram [1] with
591 a 2-s Hanning window (achieving a frequency resolution of 0.5 Hz) and 50% overlap between
592 windows. To account for the effect of notch filtering, the PSD was linearly interpolated between
593 58–62 Hz using the 10 points before and after the mentioned ranges. To analyze different
594 frequency bands, the PSD was segmented into 7 bands: delta (1–4 Hz), theta (4–8 Hz), alpha (8–

13 Hz), low beta (13–18 Hz), high beta (18–25 Hz), low gamma (25–50 Hz), and high gamma (50–100 Hz). The power within a frequency band (the area under the PSD curve for a band) was then computed for each band. The relative power in a frequency band is the ratio of the power within the band over the total power within 1–100 Hz. The normalized PSD curves were obtained by dividing the PSD curves with the total power within 1–100 Hz. The low-to-high frequency band ratio was calculated as the ratio of the total power in the alpha and beta bands (8–25 Hz) over the power in the high gamma band (50–100 Hz).

Sleep scoring

A convolutional neural network-based algorithm SPINDLE (https://sleeplearning.ethz.ch) was used for automated sleep scoring (Miladinović et al., 2019). This method produces domain invariant predictions and makes use of a hidden Markov model to limit state dynamics based on known sleep physiology. Sleep was scored from the entire second day (24 hours) of each recording. EEG signals from the frontal and somatosensory cortices and the EMG signals were used to score each 4-s epoch as wake, NREM sleep, or REM sleep. To assess the performance of this method on our dataset, two WT mice treated with control ASO, two *Ube3a*$^{m\Delta e6/p+}$ mice with control ASO, and one *Ube3a*$^{m\Delta e6/p+}$ mouse with Ube3a-as ASO were randomly selected and one hour of data from each mouse were scored by SPINDLE and manually by three experts. The Precision, Recall, F1-score, and Accuracy were calculated for each pairwise comparison as the following: $Precision = \frac{True\ positive}{True\ positive + False\ positive}$; $Recall = \frac{True\ positive}{True\ positive + False\ negative}$; $F1\text{-}score = 2 \times \frac{Precision \times Recall}{Precision + Recall}$; $Accuracy =$

616 $\frac{True\ positive+True\ negative}{True\ positive+True\ negative+False\ positive+False\ negative}$. The accuracy of SPINDLE compared to

617 experts was similar to that of the experts compared among each other (***Figure 6-supplement 1***).

618

619 **Statistics**

620 All reported sample numbers (*n*) represent independent biological replicates that are the numbers

621 of tested mice. Statistical analyses were performed with Prism 9 (GraphPad Software). Student's

622 t-test or ANOVA with multiple comparison test for all pairs of groups were used to determine if

623 there is a statistically significant difference between two groups or among three or more groups,

624 respectively. One-way or two-way ANOVA was applied for one or two independent variables,

625 respectively. Anderson-Darling test, D'Agostino-Pearson, Shapiro-Wilk, and Kolmogorov-

626 Smirnov tests were used to determine if data were normally distributed. Non-parametric Kruskal-

627 Wallis one-way ANOVA with Dunn's multiple comparison test was used for low-to-high

628 frequency band ratio and poly-spike data. The details of all statistical tests, numbers of

629 replicates, and *P* values are reported in ***Supplementary File 3***.

630

631 **Acknowledgments**

632 We thank Jacob, Debra, and Steven Sukin for inspiring this work, Baylor College of Medicine

633 Genetically Engineered Rodent Models Core led by Dr. Jason Heaney for microinjection of *Cas9*

634 mRNA and sgRNAs to generate *Ube3a*$^{\Delta e6}$ mice, and Drs. Catherine Chu, Robert Komorowski,

635 James Gilbert, Rodney Samaco, and Huda Zoghbi for discussions. This work was supported in

636 part by Texas Children's Hospital, the Eunice Kennedy Shriver National Institute of Child

637 Health and Human Development (P50HD103555 to Baylor College of Medicine Intellectual and

638 Developmental Disabilities Research Center, Neurovisualization Core), and the National Cancer

639 Institute (P30CA125123 to Baylor College of Medicine Cancer Center). MX was supported by
640 the National Institute of Neurological Disorders and Stroke (R01NS100893 and U01NS118288)
641 and the National Institute of Mental Health (R01MH117089) and is a Caroline DeLuca Scholar.
642

643 **Figures and Legends**

Figure 1

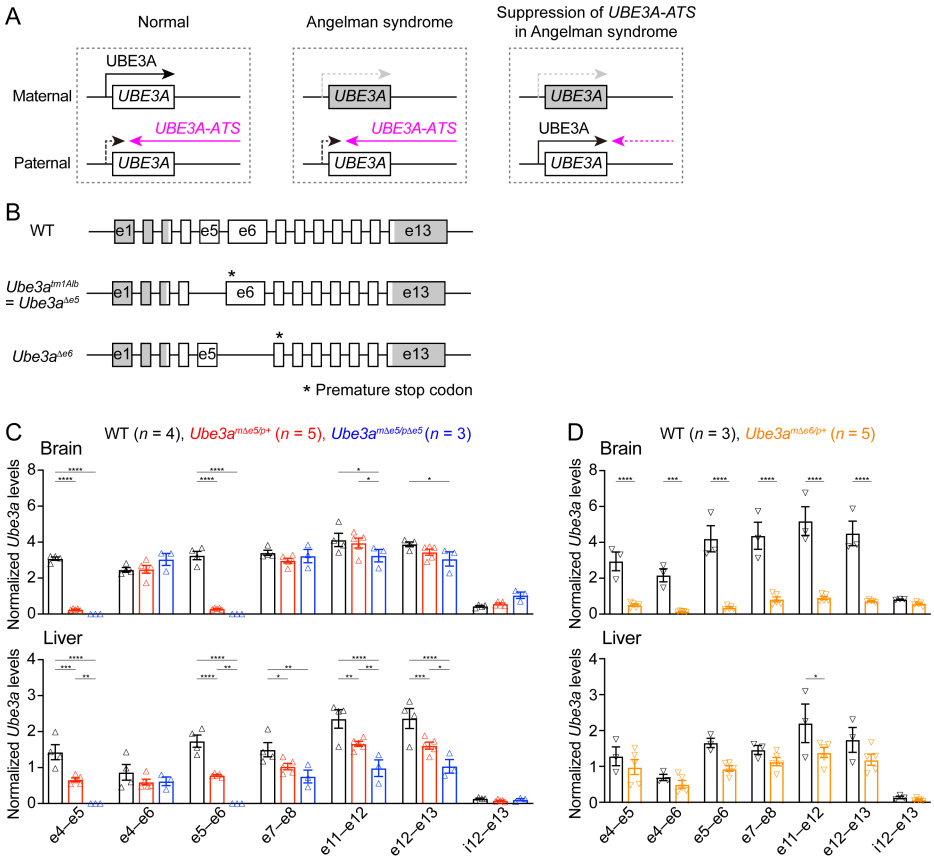

644

645 **Figure 1. *Ube3a* mRNA is diminished in the brain of a new maternal *Ube3a* knockout**

646 **mouse but remains in a previously generated Angelman syndrome mouse model.**

647 (**A**) Schematics of *UBE3A* imprinting and Angelman syndrome. Left, in normal neurons,

648 UBE3A proteins are only produced from the maternal copy of *UBE3A* because the paternal copy

649 is silenced by *UBE3A-ATS*. Middle, deficiency of the maternal *UBE3A* (grey) leads to the loss of

650 UBE3A proteins in neurons and causes Angelman syndrome. Right, suppressing *UBE3A-ATS*

651 expression leads to the unsilencing of the paternal *UBE3A*. (**B**) Genomic structures of *Ube3a*

652 WT, *Δe5* (also known as *tm1Alb*), and *Δe6* alleles. The boxes indicate exons (e) 1–13. The white

653 and grey regions indicate the coding and non-coding exon sequences of the longest *Ube3a*

654 transcript, respectively. In the *Δe5* and *Δe6* alleles, exons 5 and 6 are deleted, resulting in a
655 premature stop codon in exons 6 and 7, respectively. (**C**) *Ube3a* transcript levels were measured
656 from the brains and livers of WT, *Ube3a*$^{m\Delta e5/p+}$ and *Ube3a*$^{m\Delta e5/p\Delta e5}$ mice using primer sets
657 targeting different exons or introns as indicated in the figure. *Ube3a* levels were normalized by
658 the *Gapdh* mRNA levels. Except the deleted exon 5, other exons in the brains of *Ube3a*$^{m\Delta e5/p+}$
659 and *Ube3a*$^{m\Delta e5/p\Delta e5}$ mice remain at the similar levels as WT mice. (**D**) Similar to (C), but for WT
660 and *Ube3a*$^{m\Delta e6/p+}$ mice. *Ube3a* transcript is greatly reduced in the *Ube3a*$^{m\Delta e6/p+}$ mouse brains.
661 The numbers of tested mice are indicated in the figures. Each symbol represents one mouse. Bar
662 graphs are mean ± s.e.m. Two-way ANOVA with Tukey (C) or Šídák (D) multiple comparison
663 test for all pairs of groups, * $P < 0.05$, ** $P < 0.01$, *** $P < 0.001$, **** $P < 0.0001$.

Figure 2

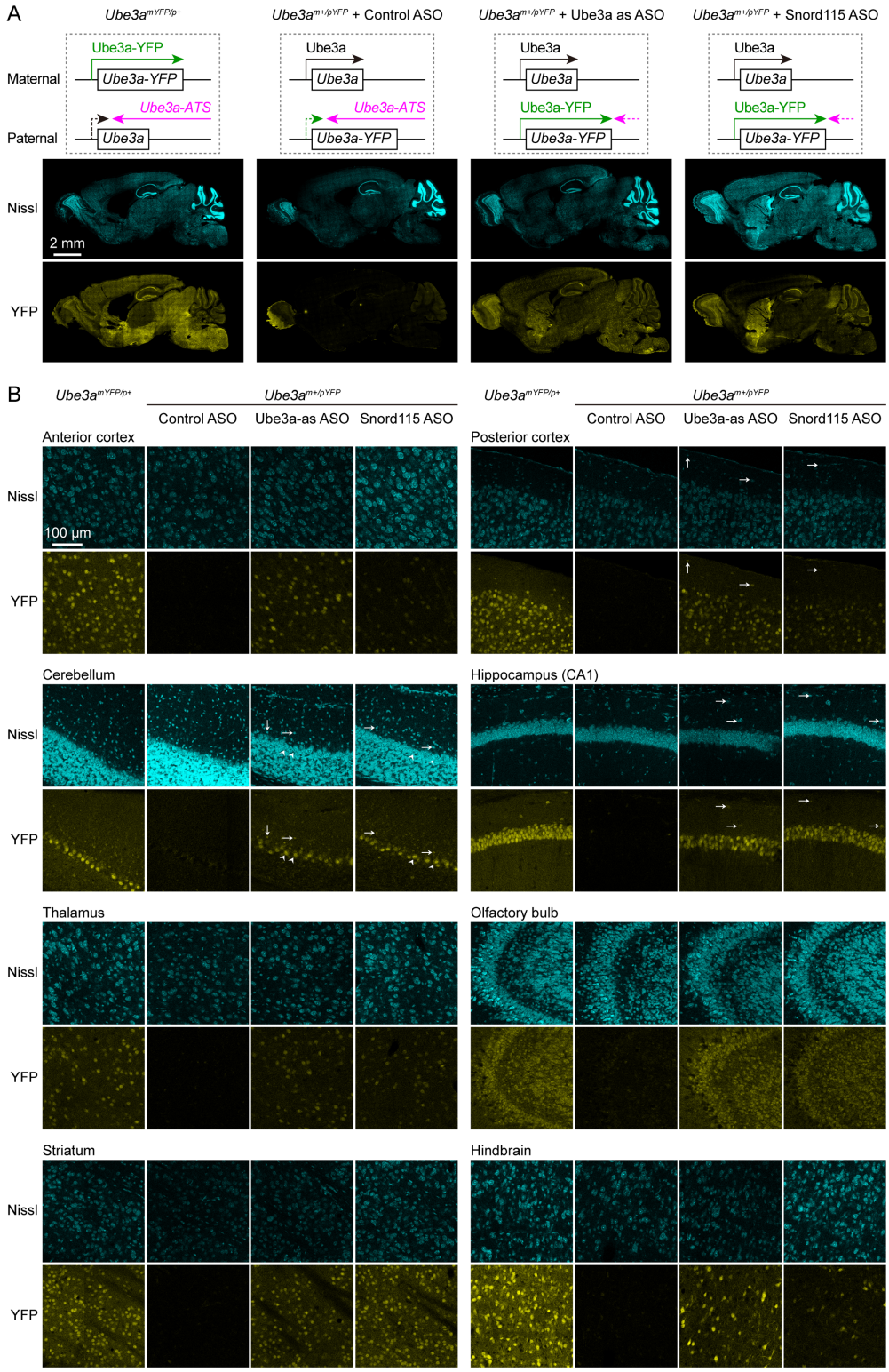

Figure 2. ASOs targeting *Ube3a-ATS* reactivate paternal *Ube3a-YFP* expression.

666 (**A**) Schematics of Ube3a-YFP expression (upper panels) and representative fluorescent images
667 of sagittal brain sections (lower panels) from maternal *Ube3a*^{YFP} mice (*Ube3a*$^{mYFP/p+}$, n = 2) and
668 paternal *Ube3a*^{YFP} mice (*Ube3a*$^{m+/pYFP}$) injected with control (n = 2), Ube3a-as (n = 2), or
669 Snord115 (n = 2) ASO. Sections were stained with fluorescent Nissl and an antibody recognizing
670 YFP. Ube3a-YFP proteins are produced from the maternal copy of *Ube3a-YFP* in *Ube3a*$^{mYFP/p+}$
671 mice, but not from the paternal copy in *Ube3a*$^{m+/pYFP}$ mice injected with control ASO because
672 the paternal copy is silenced by *Ube3a-ATS*. Both Ube3a-as and Sord115 ASOs can suppress
673 *Ube3a-ATS* expression in *Ube3a*$^{m+/pYFP}$ mice and broadly reactivate the paternal *Ube3a-YFP*
674 expression in the brains. (**B**) Similar to (A), but for images of eight different brain regions at high
675 magnification. Arrows indicate YFP positive GABAergic interneurons in cortical layer 1,
676 cerebellar molecular layer, and hippocampal stratum oriens. Arrow heads indicate YFP positive
677 cerebellar Purkinje cells.

Figure 3

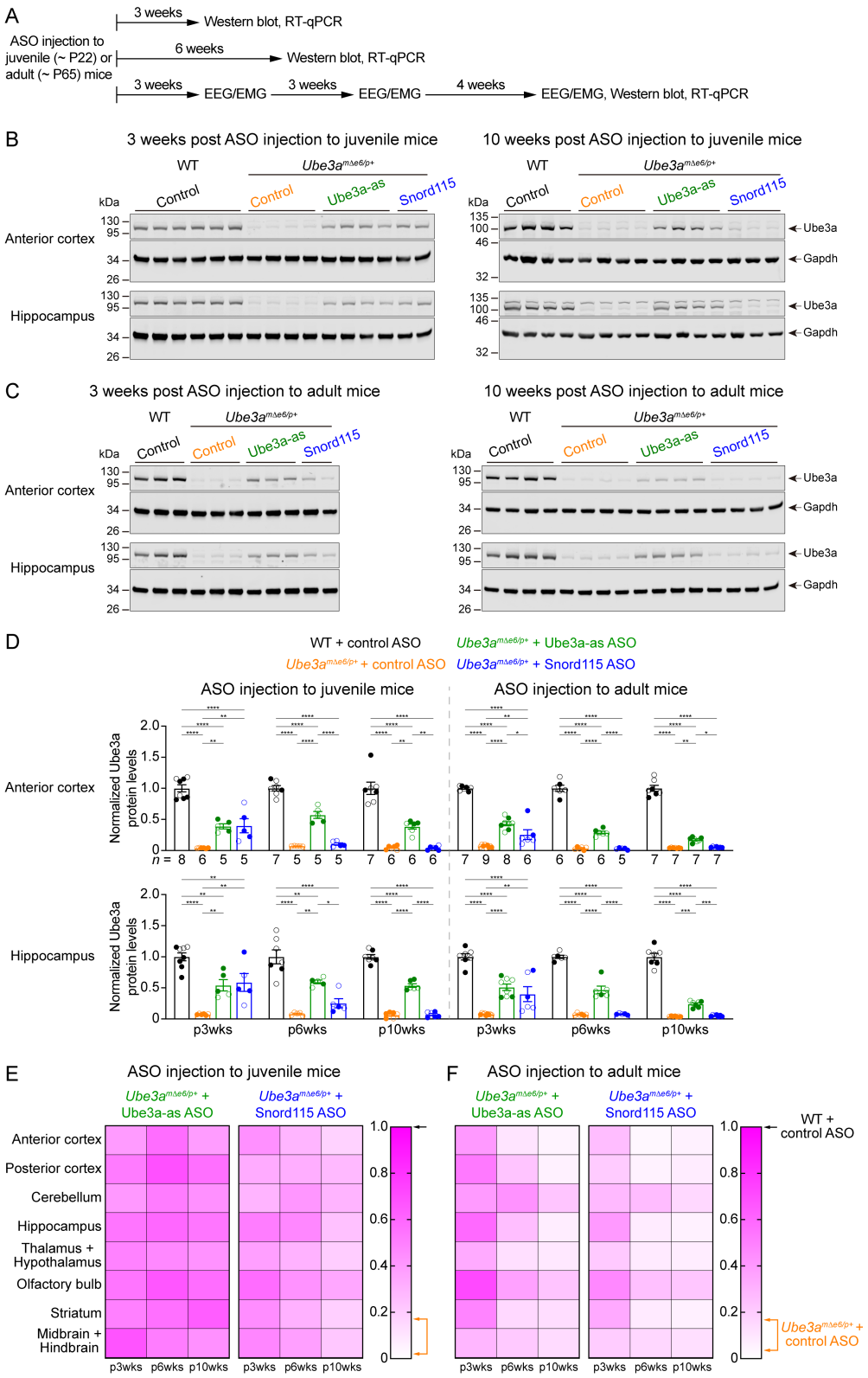
A
ASO injection to juvenile (~ P22) or adult (~ P65) mice
3 weeks
Western blot, RT-qPCR
6 weeks
Western blot, RT-qPCR
3 weeks
EEG/EMG
3 weeks
EEG/EMG
4 weeks
EEG/EMG, Western blot, RT-qPCR
B
3 weeks post ASO injection to juvenile mice
10 weeks post ASO injection to juvenile mice
WT
Ube3a m.Δe6/p+
Control
Control
Ube3a-as
Snord115
kDa
Anterior cortex
Hippocampus
Ube3a
Gapdh
C
3 weeks post ASO injection to adult mice
10 weeks post ASO injection to adult mice
D
WT + control ASO
Ube3a m.Δe6/p+ + Ube3a-as ASO
Ube3a m.Δe6/p+ + control ASO
Ube3a m.Δe6/p+ + Snord115 ASO
ASO injection to juvenile mice
ASO injection to adult mice
Normalized Ube3a protein levels
n =
p3wks
p6wks
p10wks
E
ASO injection to juvenile mice
Ube3a m.Δe6/p+ + Ube3a-as ASO
Ube3a m.Δe6/p+ + Snord115 ASO
Anterior cortex
Posterior cortex
Cerebellum
Hippocampus
Thalamus + Hypothalamus
Olfactory bulb
Striatum
Midbrain + Hindbrain
F
ASO injection to adult mice
WT + control ASO
Ube3a m.Δe6/p+ + control ASO

678

679 **Figure 3. ASOs targeting *Ube3a-ATS* up-regulate Ube3a protein in *Ube3a*$^{m\Delta e6/p+}$ mice.**

680 (**A**) Experimental designs and timelines. ASOs were injected into three cohorts of juvenile mice
681 around postnatal day 22 (P22). Protein and RNA were measured from two cohorts of mice at 3
682 and 6 weeks post ASO injection. EEG and EMG were measured from the third cohort of mice at
683 3, 6, and 10 weeks post ASO injection, and protein and RNA were measured after the last
684 EEG/EMG recording. The same experiments were performed for three cohorts of adult mice
685 injected with ASOs around P65. (**B,C**) ASOs were injected into juvenile (B) or adult (C) mice.
686 Representative Western blots at 3 and 10 weeks post ASO injection from the anterior cortex and
687 hippocampus of WT mice injected with control ASO and *Ube3a*$^{m\Delta e6/p+}$ mice with control,
688 Ube3a-as, or Snord115 ASO. Gapdh, a housekeeping protein as loading control. (**D**) Summary
689 data of normalized Ube3a protein levels from the anterior cortex (upper panel) and hippocampus
690 (lower panel) at 3, 6, and 10 weeks post ASO injection indicated by p3wks, p6wks, and p10wks,
691 respectively. Ube3a levels were first normalized by the Gapdh levels and then by the average
692 Ube3a levels of all WT mice from the same blot. Ube3a levels are diminished in control ASO-
693 treated *Ube3a*$^{m\Delta e6/p+}$ mice as compared to control ASO-treated WT mice. The up-regulation of
694 Ube3a protein by Ube3a-as ASO is evident up to 10 weeks post ASO injection, whereas the
695 effect of Snord115 ASO diminishes over time. The numbers of tested mice are indicated in the
696 figures. Each filled (male) or open (female) circle represents one mouse. Bar graphs are mean ±
697 s.e.m. One-way ANOVA with Tukey multiple comparison test for all pairs of groups, * $P < 0.05$,
698 ** $P < 0.01$, *** $P < 0.001$, **** $P < 0.0001$. (**E,F**) Heat maps showing the normalized Ube3a
699 protein levels from different brain regions of Ube3a-as or Snord115 ASO-treated juvenile (E)
700 and adult (F) *Ube3a*$^{m\Delta e6/p+}$ mice at 3, 6, and 10 weeks post ASO injection. In the color scales, 1
701 represents the Ube3a levels in control ASO-treated WT mice for each brain region (black

702 arrows), and the orange arrows indicate the range of Ube3a levels in control ASO-treated

703 *Ube3a*$^{m\Delta e6/p+}$ mice.

Figure 3-supplement 1

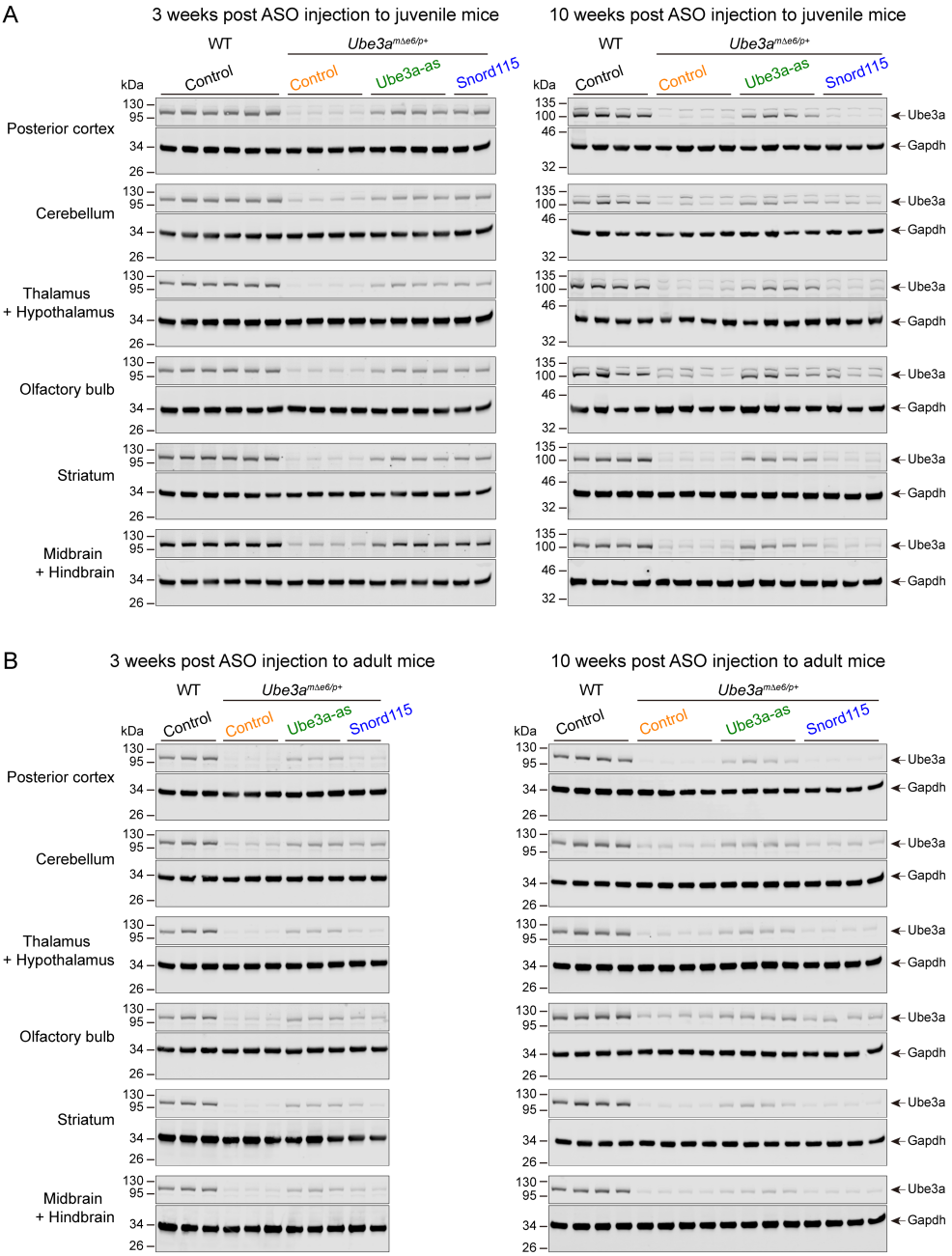

704

705 **Figure 3-supplement 1. ASOs targeting *Ube3a-ATS* up-regulate Ube3a protein in different**

706 **brain regions of *Ube3a*$^{m\Delta e6/p+}$ mice (Part I)**

707 (**A,B**) ASOs were injected into juvenile (A) or adult (B) WT and *Ube3a*$^{m\Delta e6/p+}$ mice.

708 Representative Western blots at 3 and 10 weeks post ASO injection from different brain regions

709 as indicated in the figures.

Figure 3-supplement 2

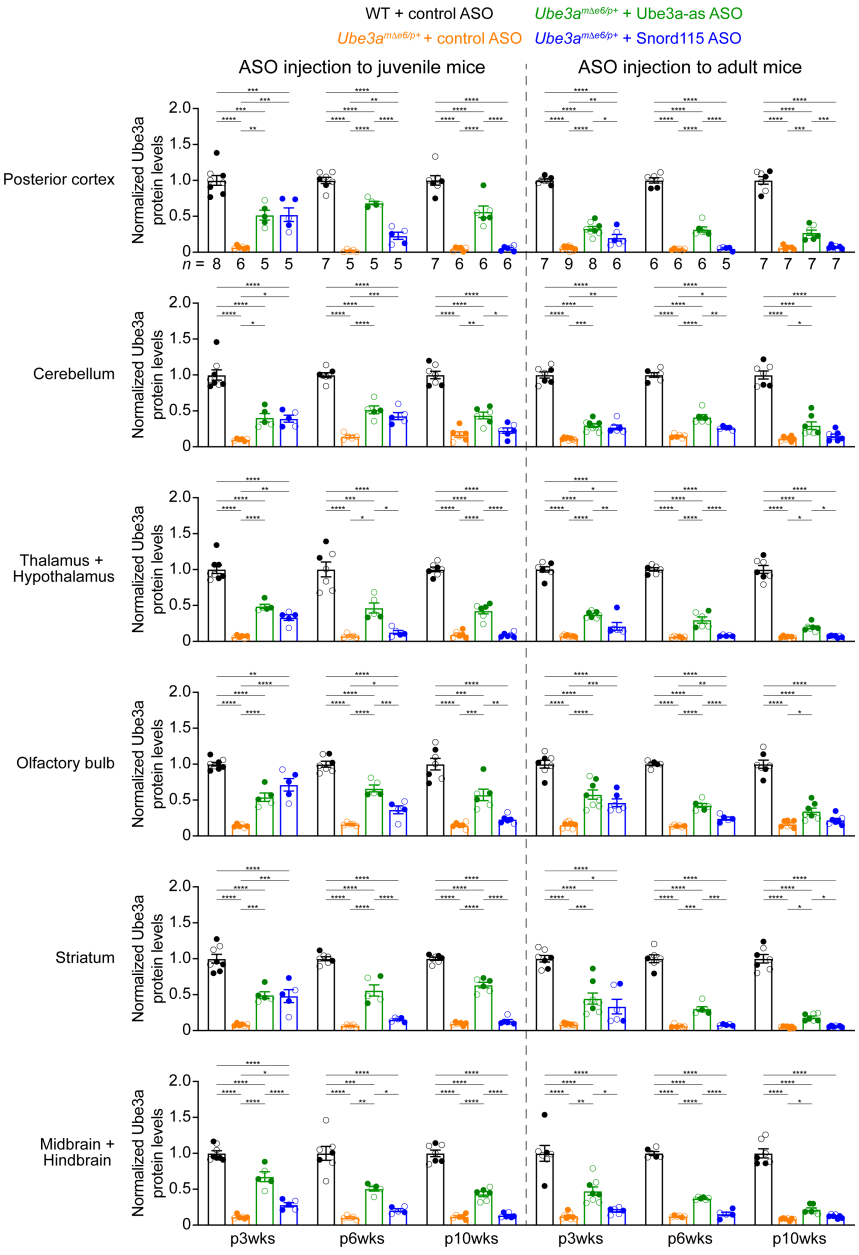

710

711 **Figure 3-supplement 2. ASOs targeting *Ube3a-ATS* up-regulate Ube3a protein in different**

712 **brain regions of *Ube3a*$^{m\Delta e6/p+}$ mice (Part II)**

713 Summary data of normalized Ube3a protein levels from different brain regions at 3, 6, and 10

714 weeks post ASO injection indicated by p3wks, p6wks, and p10wks, respectively. Ube3a levels

715 were first normalized by the Gapdh levels and then by the average Ube3a levels of all WT mice

716 from the same blot. Ube3a levels are diminished in all brain regions of control ASO-treated

717 *Ube3a*$^{m\Delta e6/p+}$ mice as compared to control ASO-treated WT mice. The up-regulation of Ube3a

718 protein by Ube3a-as ASO is evident up to 10 weeks post ASO injection, whereas the effect of

719 Snord115 ASO diminishes over time. The numbers of tested mice are indicated in the figures.

720 Each filled (male) or open (female) circle represents one mouse. Bar graphs are mean ± s.e.m.

721 One-way ANOVA with Tukey multiple comparison test for all pairs of groups, * $P < 0.05$, ** P

722 < 0.01, *** $P < 0.001$, **** $P < 0.0001$.

Figure 3-supplement 3

723 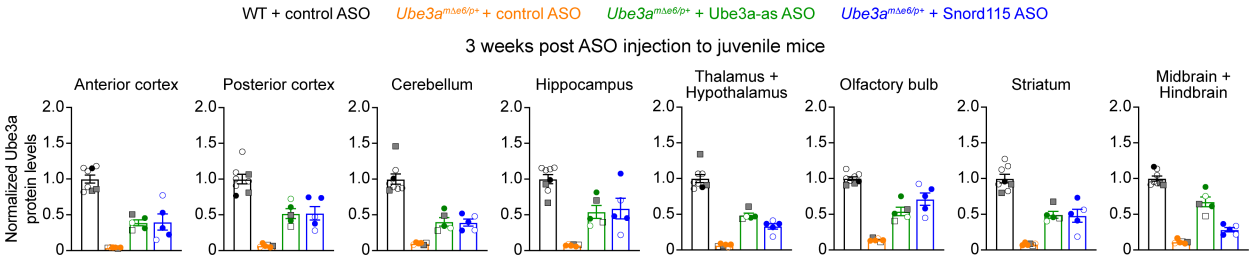

724 **Figure 3-supplement 3. Similar increase of Ube3a protein by two different doses of ASOs in**

725 ***Ube3a*$^{m\Delta e6/p+}$ mice.**

726 The same summary data presented in ***Figure 3D*** and ***Figure 3-supplement 2A*** for the

727 normalized Ube3a protein levels from 3 weeks post ASO injection into juvenile mice. The filled

728 (male) and open (female) squares represent 2 WT and 2 *Ube3a*$^{m\Delta e6/p+}$ mice injected with 250 µg

729 control ASO and 2 *Ube3a*$^{m\Delta e6/p+}$ mice with 250 µg Ube3a-as ASO. The filled (male) and open

730 (female) circle represent the rest of mice injected with 500 µg ASOs. Note the similar Ube3a

731 levels in *Ube3a*$^{m\Delta e6/p+}$ mice injected with 250 or 500 µg Ube3a-as ASO.

Figure 4

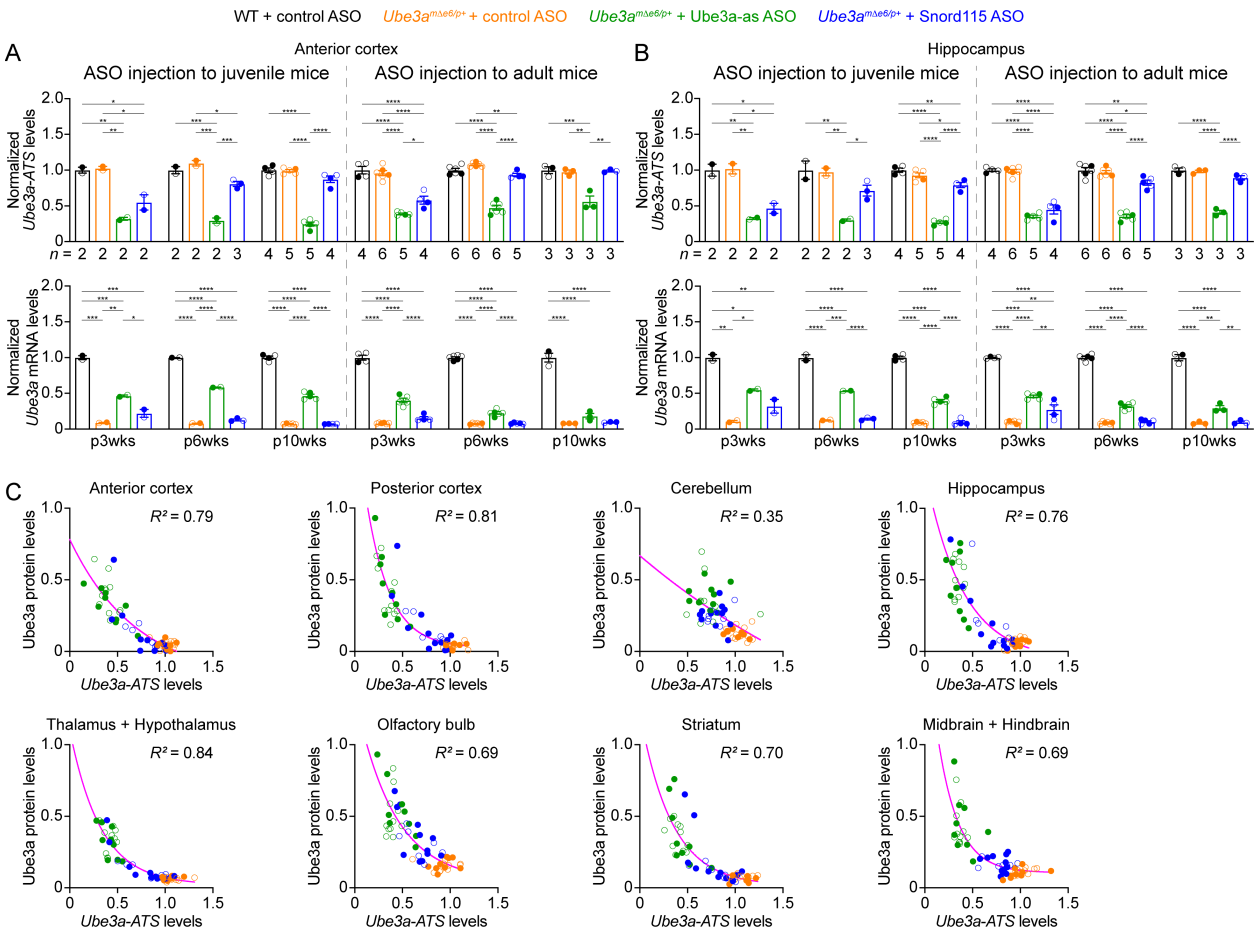

732

733 **Figure 4. ASOs targeting *Ube3a-ATS* reduce *Ube3a-ATS* and increase *Ube3a* transcripts in**

734 ***Ube3a*$^{m\Delta e6/p+}$ mice.**

735 (**A,B**) Juvenile or adult WT mice were injected with control ASO and *Ube3a*$^{m\Delta e6/p+}$ mice with

736 control, Ube3a-as, or Snord115 ASO. Summary data show the normalized *Ube3a-ATS* (upper

737 panels) and *Ube3a* (lower panels) transcript levels from the anterior cortex (A) and hippocampus

738 (B) at 3, 6, and 10 weeks post ASO injection indicated by p3wks, p6wks, and p10wks,

739 respectively. *Ube3a-ATS* and *Ube3a* levels were first normalized by the *Gapdh* levels and then

740 by the average *Ube3a-ATS* and *Ube3a* levels of all WT mice, respectively. The down-regulation
741 of *Ube3a-ATS* and up-regulation of *Ube3a* mRNA by Ube3a-as ASO is evident up to 10 weeks
742 post ASO injection, whereas the effect of Snord115 ASO diminishes over time. The numbers of
743 tested mice are indicated in the figures. Bar graphs are mean ± s.e.m. One-way ANOVA with
744 Tukey multiple comparison test for all pairs of groups, * $P < 0.05$, ** $P < 0.01$, *** $P < 0.001$,
745 **** $P < 0.0001$. (**C**) The negative correlations between *Ube3a-ATS* transcript levels and Ube3a
746 protein levels from different brain regions of $Ube3a^{m\Delta e6/p+}$ mice injected with control, Ube3a-as,
747 or Snord115 ASO were fitted with a one phase exponential decay ($Y = ae^{-kX} + b$; X, *Ube3a-*
748 *ATS* transcript levels; Y, Ube3a protein levels; a, b, k, constants). Data from 3, 6, and 10 weeks
749 post ASO injection into juvenile and adult mice were all included. Each filled (male) or open
750 (female) circle represents one mouse. R^2 indicates the goodness of fit.

Figure 4-supplement 1

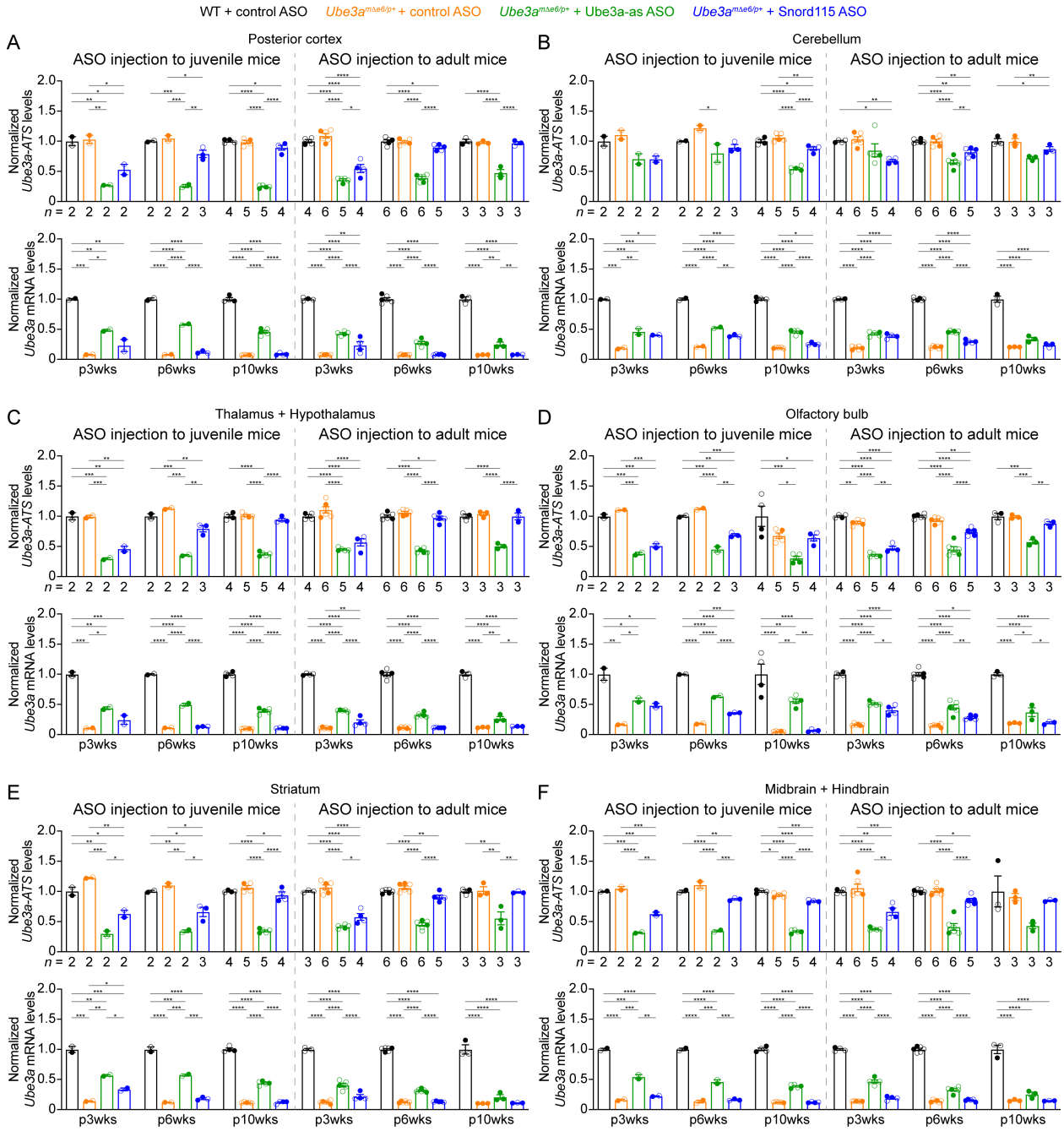

751

752 **Figure 4-supplement 1. ASOs targeting *Ube3a-ATS* reduce *Ube3a-ATS* and increase *Ube3a***

753 **transcripts in different brain regions of *Ube3a*$^{m\Delta e6/p+}$ mice (Part I).**

754 (**A–F**) Juvenile or adult WT mice were injected with control ASO and *Ube3a*$^{m\Delta e6/p+}$ mice with

755 control, Ube3a-as, or Snord115 ASO. Summary data from different brain regions show the
756 normalized *Ube3a-ATS* (upper panels) and *Ube3a* (lower panels) transcript levels at 3, 6, and 10
757 weeks post ASO injection indicated by p3wks, p6wks, and p10wks, respectively. *Ube3a-ATS*
758 and *Ube3a* levels were first normalized by the *Gapdh* levels and then by the average *Ube3a-ATS*
759 and *Ube3a* levels of all WT mice, respectively. The down-regulation of *Ube3a-ATS* and up-
760 regulation of *Ube3a* mRNA by Ube3a-as ASO is evident in different brain regions up to 10
761 weeks post ASO injection, whereas the effect of Snord115 ASO diminishes over time. The
762 numbers of tested mice are indicated in the figures. Each filled (male) or open (female) circle
763 represents one mouse. Bar graphs are mean ± s.e.m. One-way ANOVA with Tukey multiple
764 comparison test for all pairs of groups, * $P < 0.05$, ** $P < 0.01$, *** $P < 0.001$, **** $P < 0.0001$.

Figure 4-supplement 2

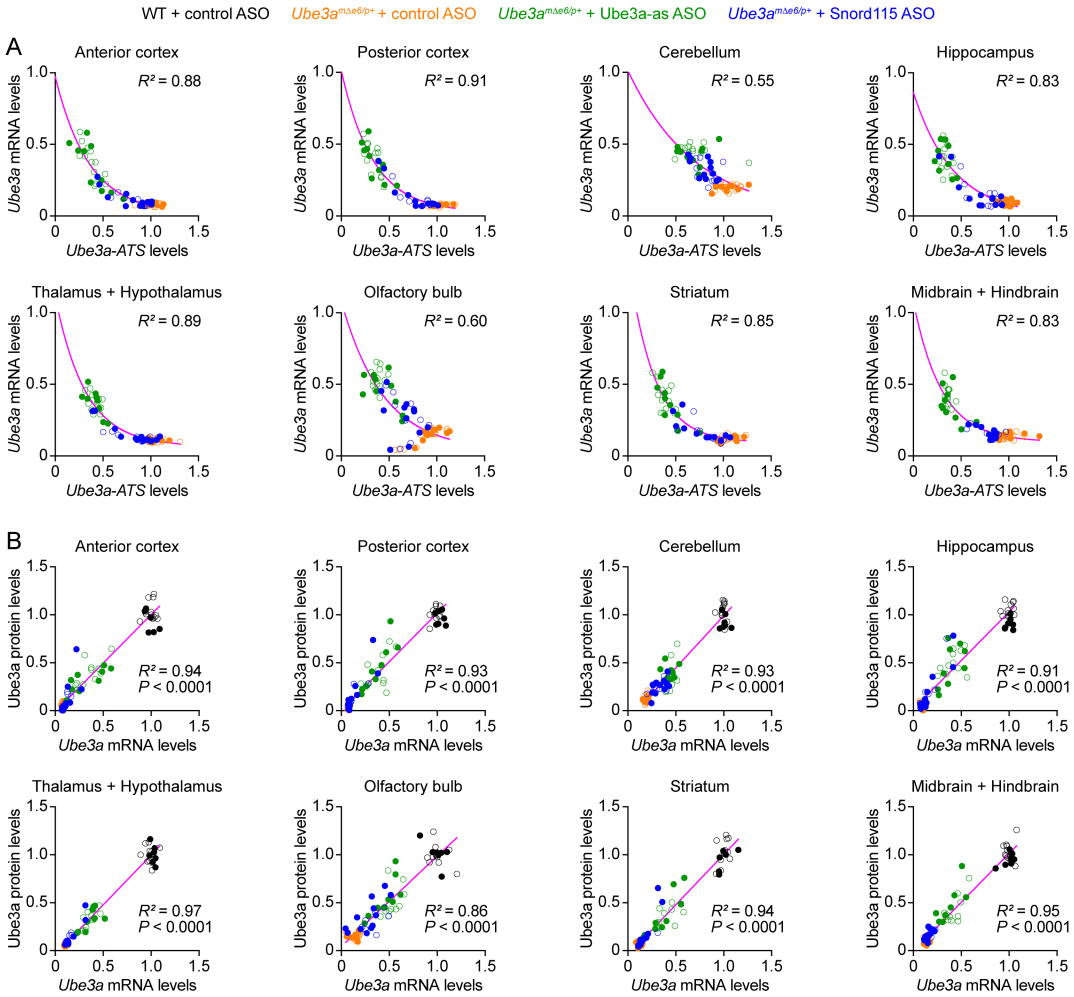

Figure 4-supplement 2. ASOs targeting *Ube3a-ATS* reduce *Ube3a-ATS* and increase *Ube3a* transcripts in different brain regions of *Ube3a*$^{m\Delta e6/p+}$ mice (Part II).

(**A**) The negative correlations between *Ube3a-ATS* transcript levels and *Ube3a* mRNA levels from different brain regions of *Ube3a*$^{m\Delta e6/p+}$ mice injected with control, Ube3a-as, or Snord115 ASO were fitted with a one phase exponential decay ($Y = ae^{-kX} + b$; X, *Ube3a-ATS* transcript levels; Y, *Ube3a* mRNA levels; a, b, k, constants). (**B**) The positive correlations between *Ube3a* mRNA levels and Ube3a protein levels from different brain regions of WT mice injected with control ASO and *Ube3a*$^{m\Delta e6/p+}$ mice with control, Ube3a-as, or Snord115 ASO were fitted with a

774 linear regression ($Y = aX + b$; X, *Ube3a* mRNA levels; Y, Ube3a protein levels; a, b, constants).

775 Data from 3, 6, and 10 weeks post ASO injection into juvenile and adult mice were all included.

776 Each filled (male) or open (female) circle represents one mouse. R^2 indicates the goodness of fit.

777 $P < 0.05$ indicates a significant deviation of slope from zero.

Figure 5

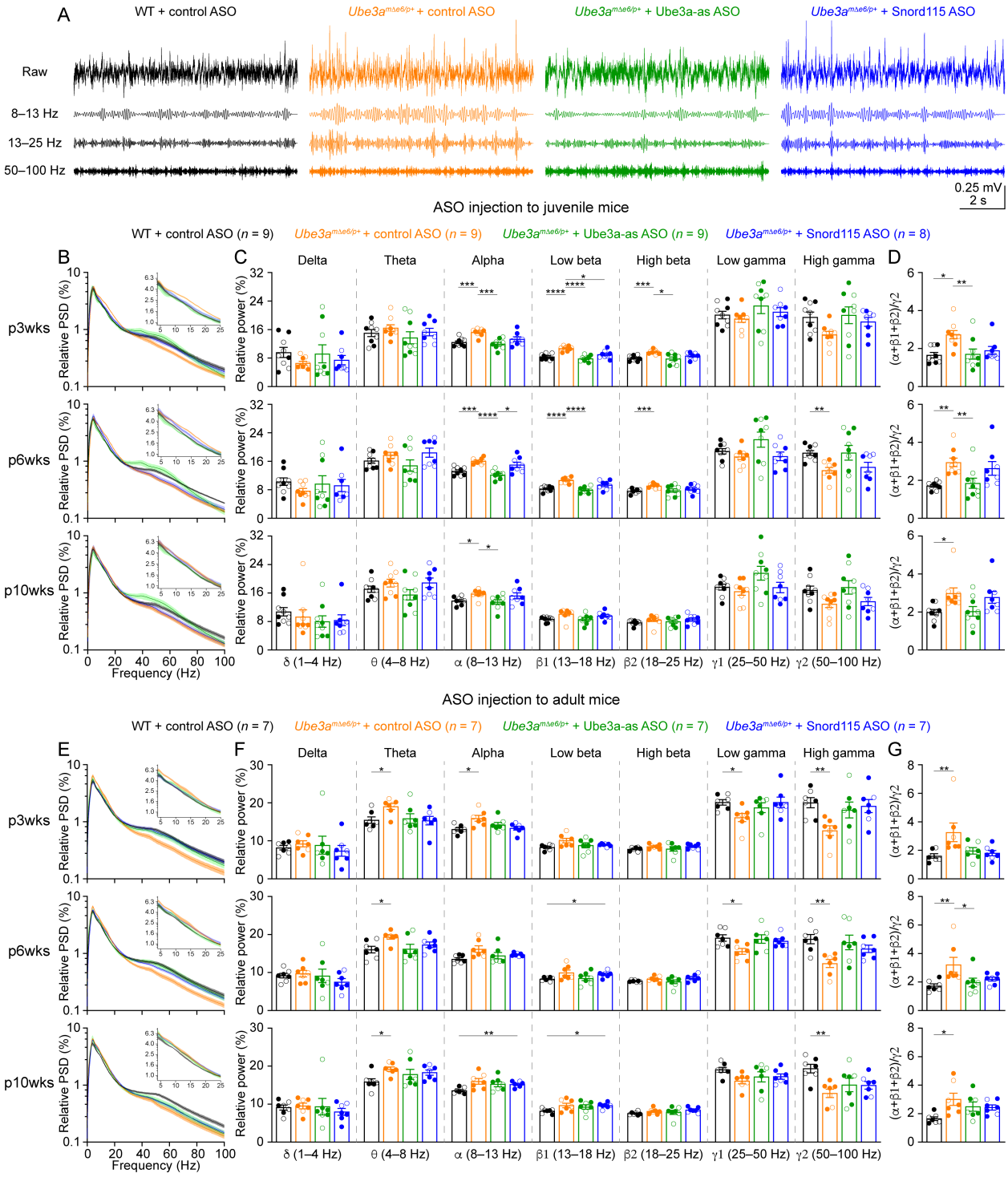

Figure 5. Reactivation of paternal *Ube3a* rescues abnormal EEG rhythms in *Ube3a$^{m\Delta e6/p+}$* mice.

781 (**A**) Juvenile WT mice were injected with control ASO and *Ube3a*$^{m\Delta e6/p+}$ mice with control,
782 Ube3a-as, or Snord115 ASO. Representative raw EEG traces and their band-pass filtered traces
783 from the left frontal cortices at 6 weeks post ASO injection. (**B**) Relative EEG power spectral
784 density (PSD) curves from the left front cortices at 3, 6, and 10 weeks post ASO injection
785 indicated by p3wks, p6wks, and p10wks, respectively. The insets show the relative PSDs in 4–25
786 Hz. Lines and shades are mean and s.e.m., respectively. (**C**) Summary data show the relative
787 power in each of the frequency bands indicated in the figure. Control ASO-treated *Ube3a*$^{m\Delta e6/p+}$
788 mice show an increase of power in the 8–25 Hz range and a decrease of power in the 50–100 Hz
789 range as compared to control ASO-treated WT mice. Ube3a-as ASO reduces the power in 8–25
790 Hz and increases the power in 50–100 Hz in *Ube3a*$^{m\Delta e6/p+}$ mice. Snord115 ASO has a similar
791 effect in *Ube3a*$^{m\Delta e6/p+}$ mice at 3 weeks post ASO injection. (**D**) Summary data show the ratio of
792 power in 8–25 Hz over 50–100 Hz. Control ASO-treated *Ube3a*$^{m\Delta e6/p+}$ mice show a higher ratio
793 than control ASO-treated WT mice. Ube3a-as ASO reduces the ratio in *Ube3a*$^{m\Delta e6/p+}$ mice.
794 Snord115 ASO has a similar effect at 3 weeks post ASO injection. (**E**–**G**) Similar to (B–D), but
795 for ASO injection into adult mice. Note, Ube3a-as ASO reduces the ratio of power in 8–25 Hz
796 over 50–100 Hz in *Ube3a*$^{m\Delta e6/p+}$ mice. The numbers of tested mice are indicated in the figures.
797 Each filled (male) or open (female) circle represents one mouse. Bar graphs are mean ± s.e.m.
798 Two-way ANOVA with Tukey multiple comparison test (C,F) and Kruskal-Wallis test with
799 Dunn's multiple comparison test (D,G) for all pairs of groups, * $P < 0.05$, ** $P < 0.01$, *** $P <$
800 0.001, **** $P < 0.0001$.

Figure 5-supplement 1

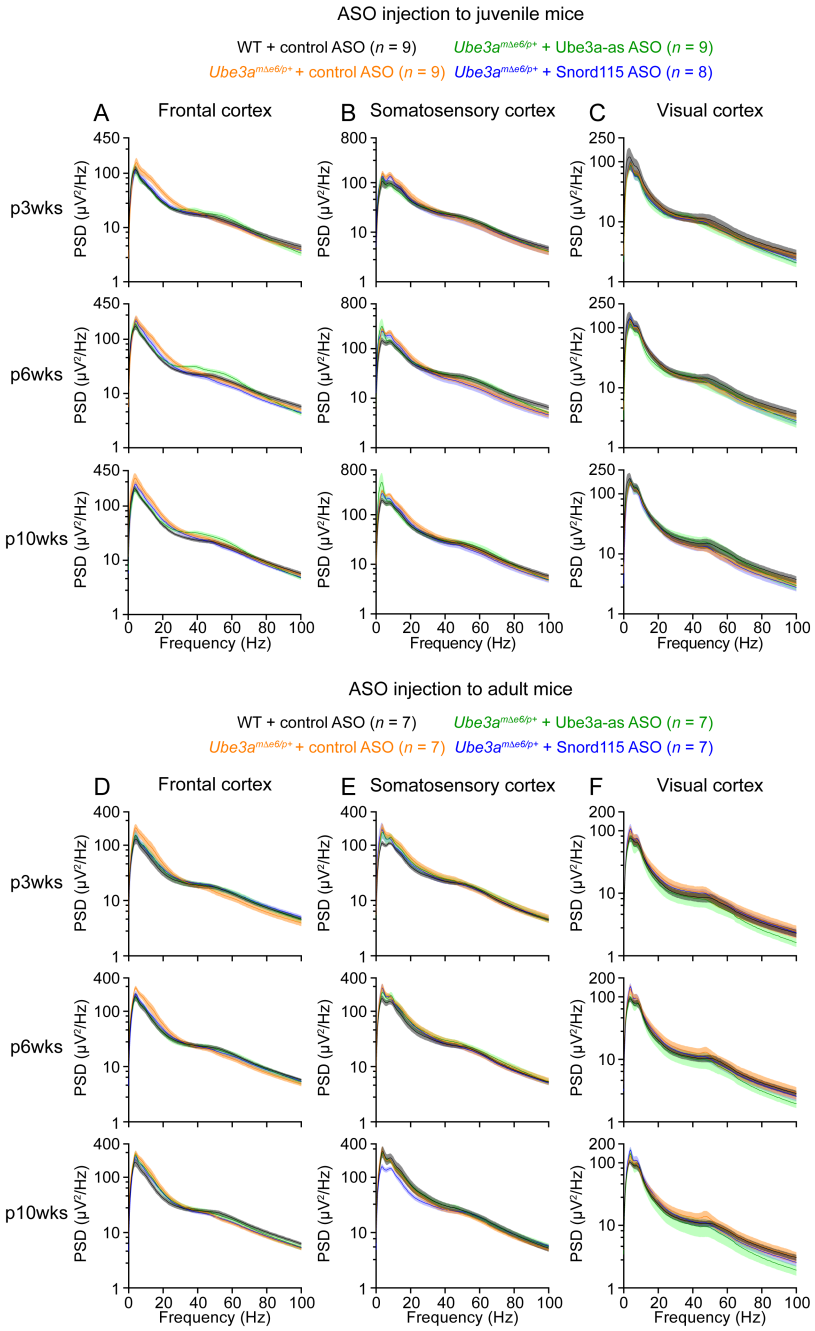

Figure 5-supplement 1. Absolute power spectral densities of EEG signals from different brain regions.

(**A–C**) EEG power spectral density (PSD) curves from the left front cortices (A), left somatosensory cortices (B), and right visual cortices (C) at 3, 6, and 10 weeks post ASO

injection into juvenile mice. (**D**–**F**) Similar to (A–C), but for ASO injection into adult mice. The numbers of tested mice are indicated in the figures. Lines and shades are mean and s.e.m., respectively.

Figure 5-supplement 2

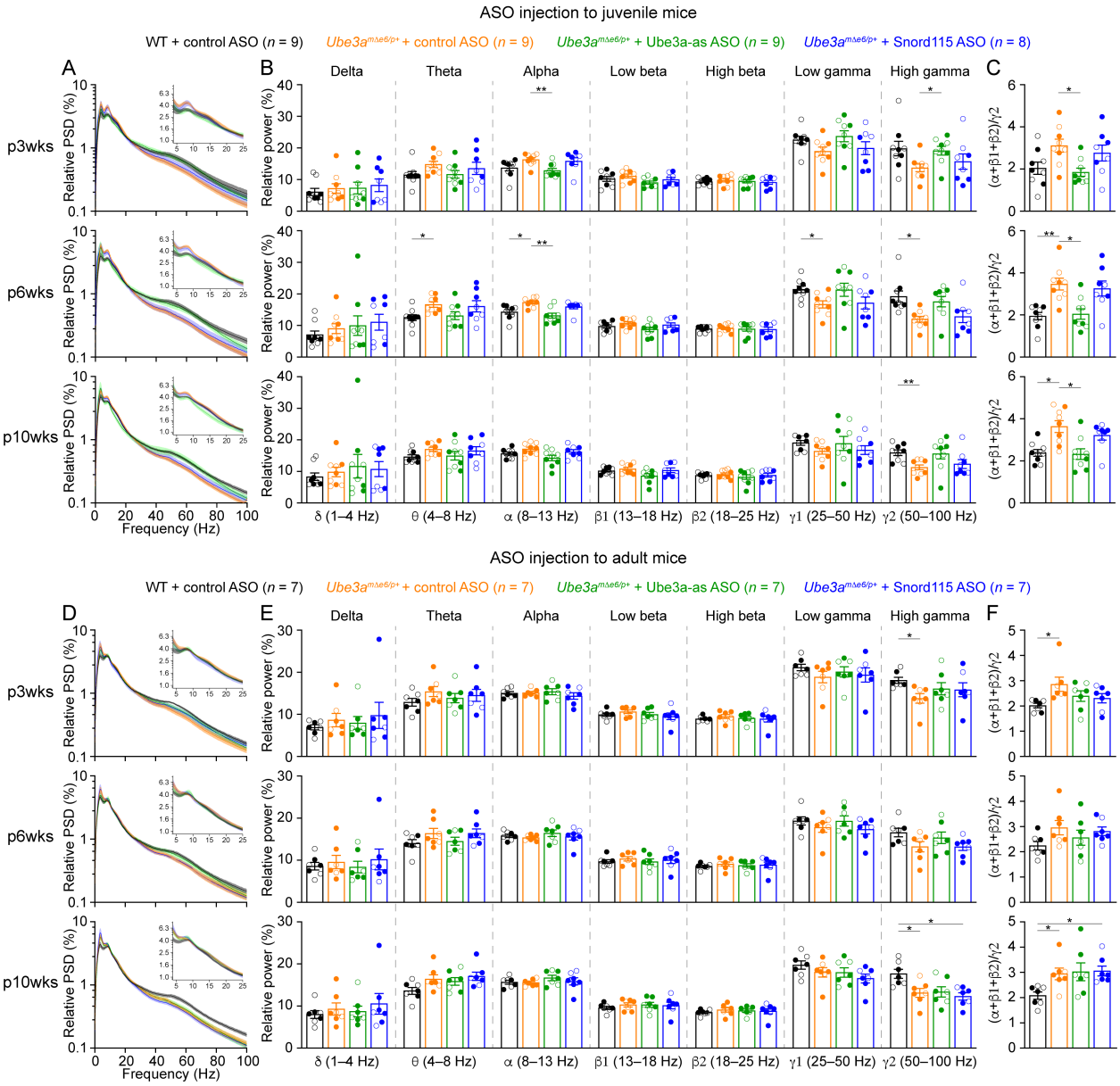

Figure 5-supplement 2. Reactivation of paternal *Ube3a* rescues abnormal EEG rhythms in the somatosensory cortex of *Ube3a*$^{m\Delta e6/p+}$ mice.

812 (**A**) Relative EEG power spectral density (PSD) curves from the left somatosensory cortices at 3,
813 6, and 10 weeks post ASO injection into juvenile mice. The insets show the relative PSDs in 4–
814 25 Hz. Lines and shades are mean and s.e.m., respectively. (**B**) Summary data show the relative
815 power in each of the frequency bands indicated in the figure. (**C**) Summary data show the ratio of
816 power in 8–25 Hz over 50–100 Hz. Control ASO-treated *Ube3a*$^{m\Delta e6/p+}$ mice show a higher ratio
817 than control ASO-treated WT mice. Ube3a-as ASO, but not Snord115 ASO, reduces the ratio
818 when injected into juvenile *Ube3a*$^{m\Delta e6/p+}$ mice. (**D**–**F**) Similar to (A–C), but for ASO injection
819 into adult mice. The numbers of tested mice are indicated in the figures. Each filled (male) or
820 open (female) circle represents one mouse. Bar graphs are mean ± s.e.m. Two-way ANOVA
821 with Tukey multiple comparison test (B,E) and Kruskal-Wallis test with Dunn's multiple
822 comparison test (C,F) for all pairs of groups, * $P < 0.05$, ** $P < 0.01$.

Figure 5-supplement 3

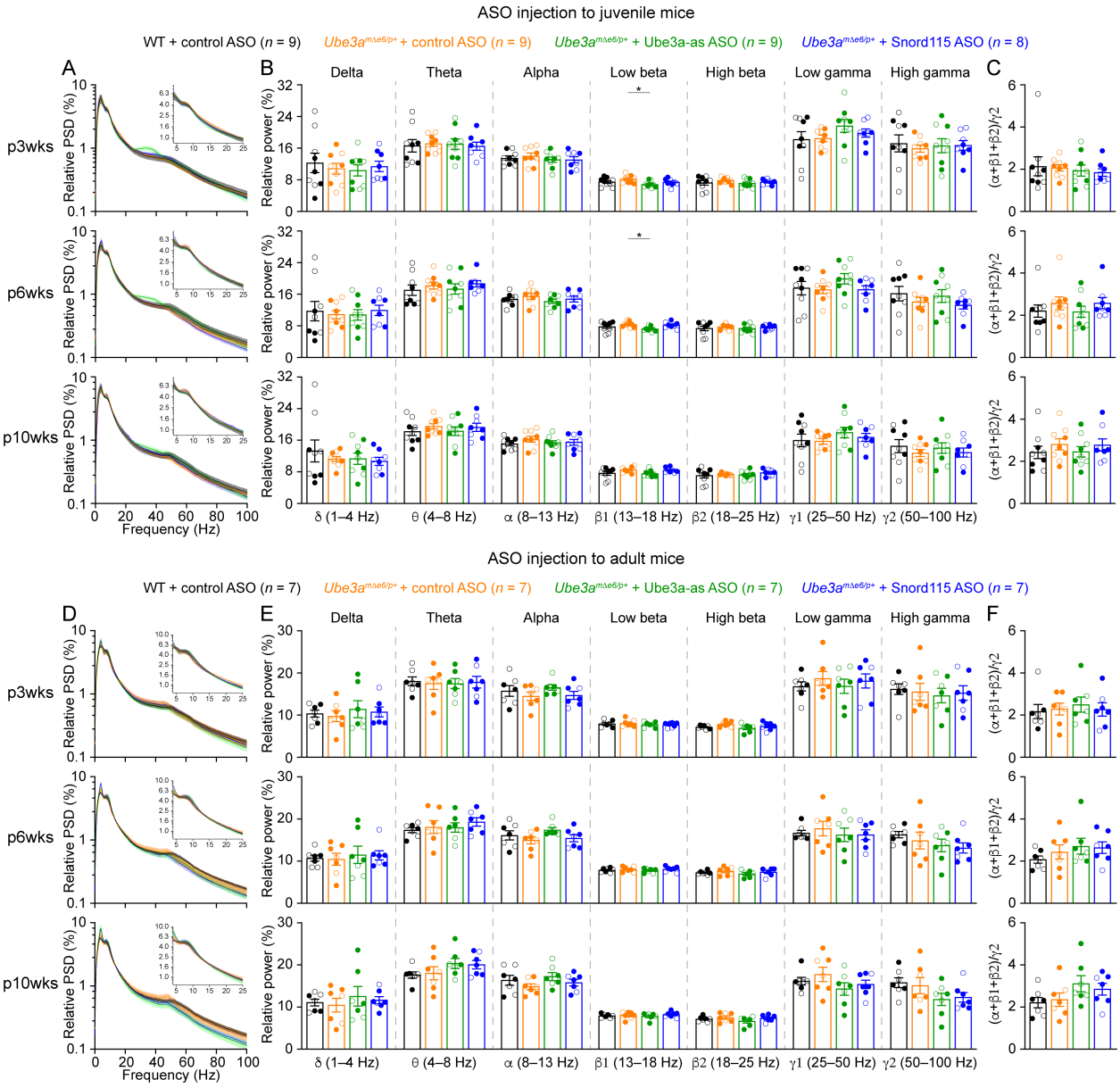

Figure 5-supplement 3. Normal EEG rhythms in the visual cortex of *Ube3a*$^{m\Delta e6/p+}$ mice. (**A**) Relative EEG power spectral density (PSD) curves from the right visual cortices at 3, 6, and 10 weeks post ASO injection into juvenile mice. The insets show the relative PSDs in 4–25 Hz. Lines and shades are mean and s.e.m., respectively. (**B**) Summary data show the relative power in each of the frequency bands indicated in the figure. (**C**) Summary data show the ratio of power

829 in 8–25 Hz over 50–100 Hz. (**D**–**F**) Similar to (A–C), but for ASO injection into adult mice. The
830 numbers of tested mice are indicated in the figures. Each filled (male) or open (female) circle
831 represents one mouse. Bar graphs are mean ± s.e.m. Two-way ANOVA with Tukey multiple
832 comparison test (B,E) and Kruskal-Wallis test with Dunn's multiple comparison test (C,F) for all
833 pairs of groups, * $P < 0.05$.

Figure 6

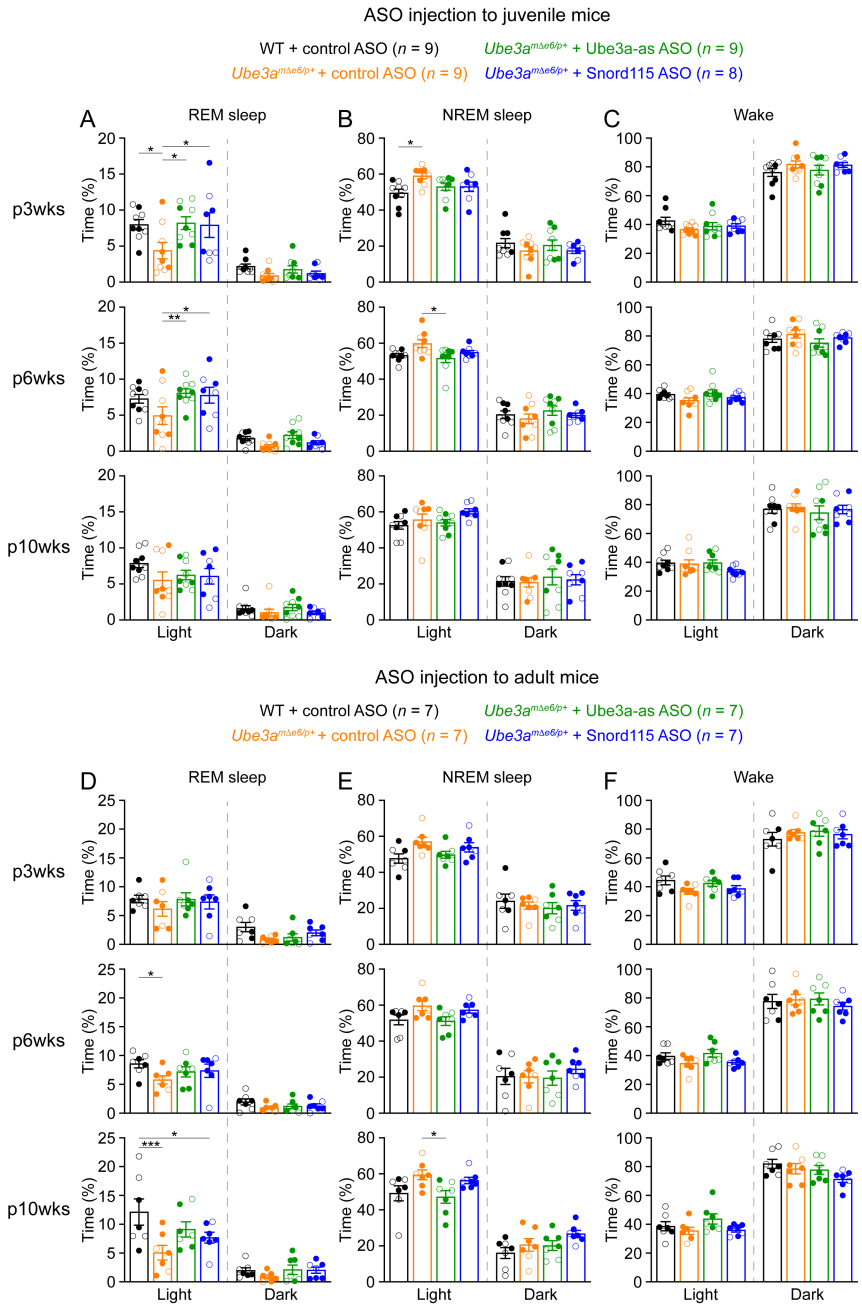

834

835 **Figure 6. Reactivation of paternal *Ube3a* rescues abnormal REM sleep in *Ube3a*$^{m\Delta e6/p+}$**

836 **mice.**

837 (**A**) Summary data of the cumulative REM sleep time at 3, 6, and 10 weeks post ASO injection

838 into juvenile mice. Control ASO-treated *Ube3a*$^{m\Delta e6/p+}$ mice spend less time in REM sleep than

839 control ASO-treated WT mice. Both Ube3a-as and Snord115 ASOs improve REM sleep in

840 *Ube3a*$^{m\Delta e6/p+}$ mice. (**B,C**) Similar to (A), but for NREM sleep (B) and wake (C). (**D–F**) Similar

841 to (A–C), but for ASO injection into adult mice. The rescue effect of Ube3a-as and Snord115

842 ASOs is reduced as compare to ASO injection into juvenile mice. The numbers of tested mice

843 are indicated in the figures. Each filled (male) or open (female) circle represents one mouse. Bar

844 graphs are mean ± s.e.m. Two-way ANOVA with Tukey multiple comparison test for all pairs of

845 groups, * $P < 0.05$, ** $P < 0.01$, *** $P < 0.001$.

Figure 6-supplement 1

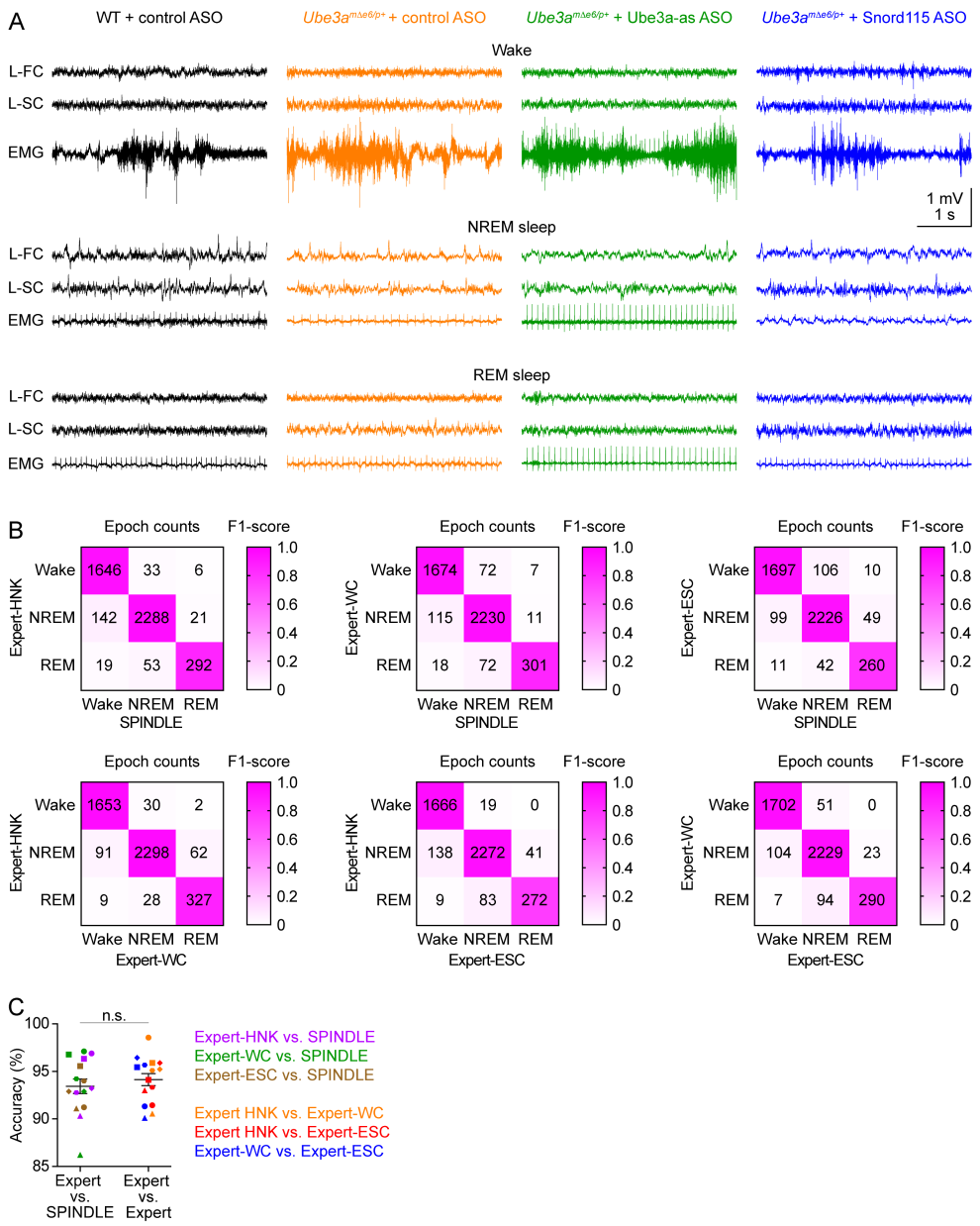

Figure 6-supplment 1. Validation of sleep staging by SPINDLE program.

(**A**) Representative EEG traces from the left frontal cortices (L-FC) and left somatosensory cortices (L-SC), and EMG traces from the neck muscles during wake (top panels), NREM sleep (middle panels), and REM sleep (bottom panels) at 3 weeks post ASO injection into juvenile mice. (**B**) The wake, NREM sleep, and REM sleep of five mice (two WT mice injected with

852 control ASO, two *Ube3a*$^{m\Delta e6/p+}$ mice with control ASO, and one *Ube3a*$^{m\Delta e6/p+}$ mouse with

853 Ube3a-as ASO, 1 hour of data from each mouse) were determined by SPINDLE program and

854 three human experts (HNK, WC, ESC). The matrices compare the epoch counts of wake, NREM

855 sleep, and REM sleep between SPINDLE and experts (upper panels) and between experts (low

856 panels). The colors indicate the F1-score. (**C**) The accuracy of sleep staging between SPINDLE

857 and experts is similar to that between experts. The symbol color represents a pair of comparisons

858 as indicated in the figure, and the symbol shape represents a mouse. Line graphs are mean ±

859 s.e.m. Unpaired t-test with Welch's correction (two-tailed), n.s., $P = 0.5$.

Figure 7

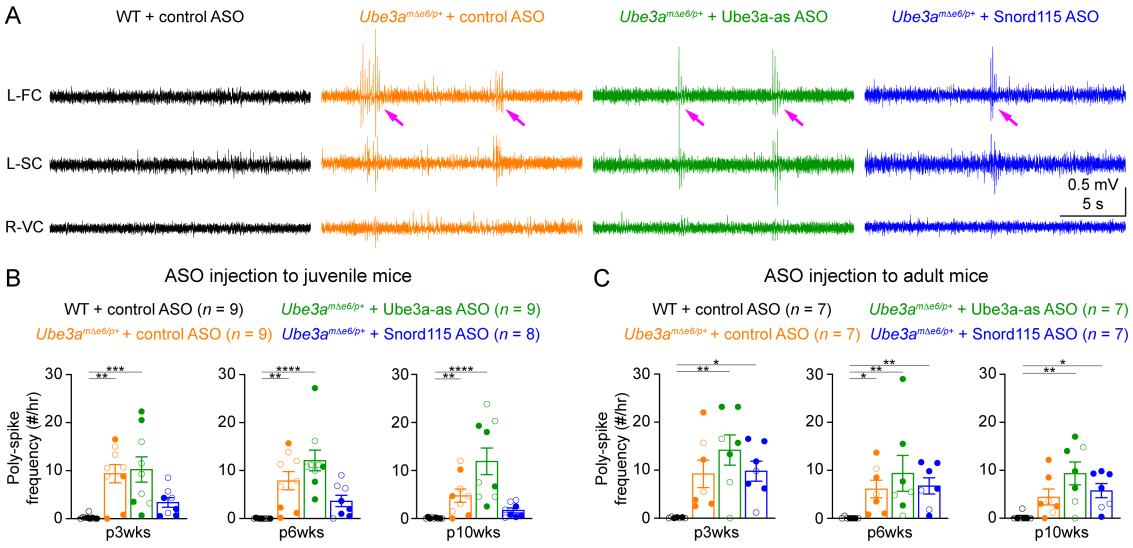

860

861 **Figure 7. Reactivation of paternal *Ube3a* does not suppress poly-spikes in *Ube3a*$^{m\Delta e6/p+}$**

862 **mice.**

863 (**A**) Representative EEG traces from the left frontal cortices (L-FC), left somatosensory cortices

864 (L-SC), and right visual cortices (R-VC) at 3 weeks post ASO injection into juvenile mice. (**B**)

865 Summary data showing the frequencies of poly-spikes from the left frontal cortices at 3, 6, and

866 10 weeks post ASO injection into juvenile mice. Control ASO-treated *Ube3a*$^{m\Delta e6/p+}$ mice show

867 many more poly-spikes than control ASO-treated WT mice. Snord115 ASO modestly reduces
868 poly-spikes, whereas Ube3a-as ASO does not. (**C**) Similar to (B), but for ASO injection into
869 adult mice. Neither Ube3a-as or Snord115 reduces poly-spikes. The numbers of tested mice are
870 indicated in the figures. Each filled (male) or open (female) circle represents one mouse. Bar
871 graphs are mean ± s.e.m. Kruskal-Wallis test with Dunn's multiple comparison test for all pairs
872 of groups, * $P < 0.05$, ** $P < 0.01$, *** $P < 0.001$, **** $P < 0.0001$.

Figure 7-supplement 1

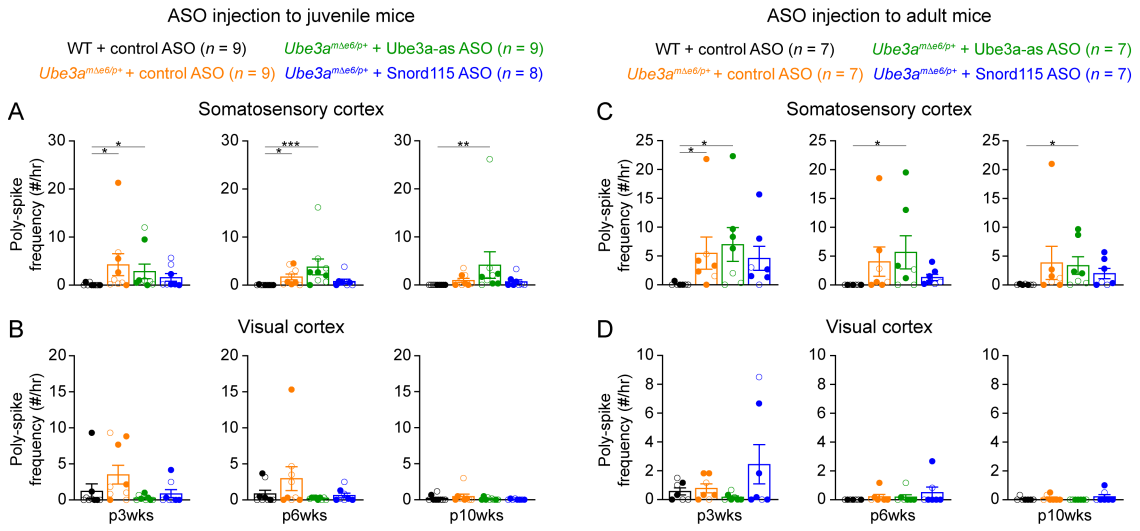

873

874 **Figure 7-supplement 1. Poly-spikes in the somatosensory and visual cortices of *Ube3a*$^{m\Delta e6/p+}$**
875 **mice.**

876 (**A**) Summary data showing the frequencies of poly-spikes from the left somatosensory cortices
877 at 3, 6, and 10 weeks post ASO injection into juvenile mice. Control ASO-treated *Ube3a*$^{m\Delta e6/p+}$
878 mice show more poly-spikes than control ASO-treated WT mice. Snord115 ASO modestly
879 reduces poly-spikes, whereas Ube3a-as ASO does not. (**B**) Similar to (A), but for the visual
880 cortices. The frequencies of poly-spikes are not significantly increased in control ASO-treated
881 *Ube3a*$^{m\Delta e6/p+}$ mice as compared to control ASO-treated WT mice. (**C,D**) Similar to (A,B), but for

882 ASO injection into adult mice. Neither Ube3a-as or Snord115 reduces poly-spikes in the
883 somatosensory cortices. The numbers of tested mice are indicated in the figures. Each filled
884 (male) or open (female) circle represents one mouse. Bar graphs are mean ± s.e.m. Kruskal-
885 Wallis test with Dunn's multiple comparison test for all pairs of groups, * $P < 0.05$, ** $P < 0.01$,
886 *** $P < 0.001$.

Figure 8

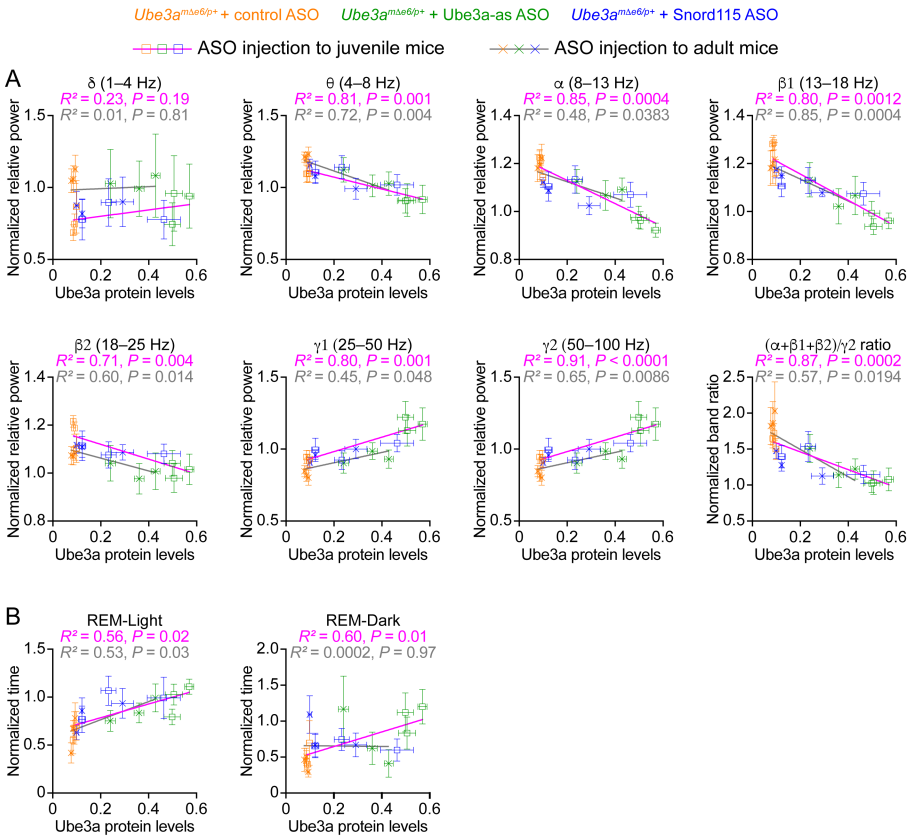

887

888 **Figure 8. EEG rhythms and REM sleep correlate with Ube3a protein levels in *Ube3a$^{m\Delta e6/p+}$***
889 **mice.**

890 (**A**) The relationships between the Ube3a protein levels and EEG relative power from the frontal
891 cortices of *Ube3a$^{m\Delta e6/p+}$* mice injected with control, Ube3a-as, or Snord115 ASO across 3, 6, and
892 10 weeks post ASO injection into juvenile and adult mice. The Ube3a protein levels from all

893 brain regions were averaged for each mouse. The relative EEG power within each frequency
894 band and the power ratio (α+β1+β2)/γ2 were normalized by the means of those in WT mice
895 injected with control ASO. The relationships were fitted with a linear regression ($Y = aX + b$; X,
896 Ube3a protein levels; Y, normalized EEG relative power or power ratio (α+β1+β2)/γ2; a, b,
897 constants). (**B**) Similar to (A), but for the relationships between the Ube3a protein levels and
898 REM sleep time in light and dark phases. Data are mean ± s.e.m. R^2 indicates the goodness of fit.
899 $P < 0.05$ indicates a significant deviation of slope from zero.
900
901 **Supplementary File 1. Comparison of phenotypic rescue of maternal *Ube3a* knockout mice**
902 **by restoring *Ube3a* expression at different ages**
903 The table summarizes the outcomes of restoring *Ube3a* expression in maternal *Ube3a* knockout
904 mice at different developmental ages from previous studies.
905
906 **Supplementary File 2. Primers and probes for RT-ddPCR and RT-qPCR**
907 The sequences of the primers and probes used in the RT-ddPCR or RT-qPCR experiments for
908 detecting *Ube3a*, *Ube3a-ATS*, and *Gapdh* are provided.
909
910 **Supplementary File 3. Statistics of experimental results.**
911 The details of all statistical tests, numbers of replicates, and *P* values are presented for each
912 experiment in the table.
913
914

915 **References**

916 Albrecht U, Sutcliffe JS, Cattanach BM, Beechey CV, Armstrong D, Eichele G, Beaudet AL
917 (1997) Imprinted expression of the murine Angelman syndrome gene, Ube3a, in
918 hippocampal and Purkinje neurons. Nat Genet 17:75–78.

919 Bird LM (2014) Angelman syndrome: review of clinical and molecular aspects. Appl Clin Genet
920 7:93–104.

921 Born HA, Dao AT, Levine AT, Lee WL, Mehta NM, Mehra S, Weeber EJ, Anderson AE (2017)
922 Strain-dependence of the Angelman Syndrome phenotypes in Ube3a maternal deficiency
923 mice. Sci Rep 7:8451.

924 Born HA, Martinez LA, Levine AT, Harris SE, Mehra S, Lee WL, Dindot SV, Nash KR,
925 Silverman JL, Segal DJ, Weeber EJ, Anderson AE (2021) Early Developmental EEG and
926 Seizure Phenotypes in a Full Gene Deletion of Ubiquitin Protein Ligase E3A Rat Model of
927 Angelman Syndrome. eNeuro 8.

928 Buiting K, Williams C, Horsthemke B (2016) Angelman syndrome - insights into a rare
929 neurogenetic disorder. Nat Rev Neurol 12:584–593.

930 Chen W, Cai Z-L, Chao ES, Chen H, Longley CM, Hao S, Chao H-T, Kim JH, Messier JE,
931 Zoghbi HY, Tang J, Swann JW, Xue M (2020) Stxbp1/Munc18-1 haploinsufficiency impairs
932 inhibition and mediates key neurological features of STXBP1 encephalopathy. Elife 9.

933 Colas D, Wagstaff J, Fort P, Salvert D, Sarda N (2005) Sleep disturbances in Ube3a maternal-
934 deficient mice modeling Angelman syndrome. Neurobiol Dis 20:471–478.

935 Copping NA, McTighe SM, Fink KD, Silverman JL (2021) Emerging Gene and Small Molecule
936 Therapies for the Neurodevelopmental Disorder Angelman Syndrome. Neurotherapeutics
937 18:1535–1547.

938 Copping NA, Silverman JL (2021) Abnormal electrophysiological phenotypes and sleep deficits
939 in a mouse model of Angelman Syndrome. Mol Autism 12:9–14.

940 Daily JL, Nash K, Jinwal U, Golde T, Rogers J, Peters MM, Burdine RD, Dickey C, Banko JL,
941 Weeber EJ (2011) Adeno-associated virus-mediated rescue of the cognitive defects in a
942 mouse model for Angelman syndrome. PLoS ONE 6:e27221.

943 Dindot SV, Antalffy BA, Bhattacharjee MB, Beaudet AL (2008) The Angelman syndrome
944 ubiquitin ligase localizes to the synapse and nucleus, and maternal deficiency results in
945 abnormal dendritic spine morphology. Hum Mol Genet 17:111–118.

946 Ehlen JC, Jones KA, Pinckney L, Gray CL, Burette S, Weinberg RJ, Evans JA, Brager AJ, Zylka
947 MJ, Paul KN, Philpot BD, DeBruyne JP (2015) Maternal Ube3a Loss Disrupts Sleep
948 Homeostasis But Leaves Circadian Rhythmicity Largely Intact. Journal of Neuroscience
949 35:13587–13598.

950 Elgersma Y, Sonzogni M (2021) UBE3A reinstatement as a disease-modifying therapy for
951 Angelman syndrome. Dev Med Child Neurol 63:802–807.

952 Frohlich J, Miller MT, Bird LM, Garces P, Purtell H, Hoener MC, Philpot BD, Sidorov MS, Tan
953 W-H, Hernandez M-C, Rotenberg A, Jeste SS, Krishnan M, Khwaja O, Hipp JF (2019)
954 Electrophysiological Phenotype in Angelman Syndrome Differs Between Genotypes. Biol
955 Psychiatry 85:752–759.

956 Grier MD, Carson RP, Lagrange AH (2015) Toward a Broader View of Ube3a in a Mouse
957 Model of Angelman Syndrome: Expression in Brain, Spinal Cord, Sciatic Nerve and Glial
958 Cells. PLoS ONE 10:e0124649.

959 Gu B, Carstens KE, Judson MC, Dalton KA, Rougie M, Clark EP, Dudek SM, Philpot BD
960 (2018) Ube3a reinstatement mitigates epileptogenesis in Angelman syndrome model mice. J
961 Clin Invest 129.

962 Hipp JF, Frohlich J, Keute M, Tan W-H, Bird LM (2021) Electrophysiological Abnormalities in
963 Angelman Syndrome Correlate With Symptom Severity. Biol Psychiatry Glob Open Sci
964 1:201–209.

965 Huang H-S, Allen JA, Mabb AM, King IF, Miriyala J, Taylor-Blake B, Sciaky N, Dutton JW,
966 Lee H-M, Chen X, Jin J, Bridges AS, Zylka MJ, Roth BL, Philpot BD (2011)
967 Topoisomerase inhibitors unsilence the dormant allele of Ube3a in neurons. Nature 481:185–
968 189.

969 Jiang YH, Armstrong D, Albrecht U, Atkins CM, Noebels JL, Eichele G, Sweatt JD, Beaudet AL
970 (1998) Mutation of the Angelman ubiquitin ligase in mice causes increased cytoplasmic p53
971 and deficits of contextual learning and long-term potentiation. Neuron 21:799–811.

972 Judson MC, Shyng C, Simon JM, Davis CR, Punt AM, Salmon MT, Miller NW, Ritola KD,
973 Elgersma Y, Amaral DG, Gray SJ, Philpot BD (2021) Dual-isoform hUBE3A gene transfer
974 improves behavioral and seizure outcomes in Angelman syndrome model mice. JCI Insight
975 6.

976 Judson MC, Sosa-Pagan JO, Del Cid WA, Han JE, Philpot BD (2014) Allelic specificity of
977 Ube3a expression in the mouse brain during postnatal development. J Comp Neurol
978 522:1874–1896.

979 Kishino T, Lalande M, Wagstaff J (1997) UBE3A/E6-AP mutations cause Angelman syndrome.
980 Nat Genet 15:70–73.

981 Mandel-Brehm C, Salogiannis J, Dhamne SC, Rotenberg A, Greenberg ME (2015) Seizure-like
982 activity in a juvenile Angelman syndrome mouse model is attenuated by reducing Arc
983 expression. Proc Natl Acad Sci USA 112:5129–5134.

984 Margolis SS, Sell GL, Zbinden MA, Bird LM (2015) Angelman Syndrome. Neurotherapeutics
985 12:641–650.

986 Markati T, Duis J, Servais L (2021) Therapies in preclinical and clinical development for
987 Angelman syndrome. Expert Opin Investig Drugs 30:709–720.

988 Matsuura T, Sutcliffe JS, Fang P, Galjaard RJ, Jiang YH, Benton CS, Rommens JM, Beaudet AL
989 (1997) De novo truncating mutations in E6-AP ubiquitin-protein ligase gene (UBE3A) in
990 Angelman syndrome. Nat Genet 15:74–77.

991 Meng L, Person RE, Beaudet AL (2012) Ube3a-ATS is an atypical RNA polymerase II transcript
992 that represses the paternal expression of Ube3a. Hum Mol Genet 21:3001–3012.

993 Meng L, Person RE, Huang W, Zhu PJ, Costa-Mattioli M, Beaudet AL (2013) Truncation of
994 Ube3a-ATS unsilences paternal Ube3a and ameliorates behavioral defects in the Angelman
995 syndrome mouse model. PLoS Genet 9:e1004039.

996 Meng L, Ward AJ, Chun S, Bennett CF, Beaudet AL, Rigo F (2015) Towards a therapy for
997 Angelman syndrome by targeting a long non-coding RNA. Nature 518:409–412.

998 Miano S, Bruni O, Elia M, Musumeci SA, Verrillo E, Ferri R (2005) Sleep breathing and
999 periodic leg movement pattern in Angelman Syndrome: a polysomnographic study. Clin
1000 Neurophysiol 116:2685–2692.

1001 Miano S, Bruni O, Leuzzi V, Elia M, Verrillo E, Ferri R (2004) Sleep polygraphy in Angelman
1002 syndrome. Clin Neurophysiol 115:938–945.

1003 Miladinović Đ, Muheim C, Bauer S, Spinnler A, Noain D, Bandarabadi M, Gallusser B,
1004 Krummenacher G, Baumann C, Adamantidis A, Brown SA, Buhmann JM (2019) SPINDLE:
1005 End-to-end learning from EEG/EMG to extrapolate animal sleep scoring across experimental
1006 settings, labs and species. PLoS Comput Biol 15:e1006968.

1007 Milazzo C, Mientjes EJ, Wallaard I, Rasmussen SV, Erichsen KD, Kakunuri T, van der Sman
1008 ASE, Kremer T, Miller MT, Hoener MC, Elgersma Y (2021) Antisense oligonucleotide
1009 treatment rescues UBE3A expression and multiple phenotypes of an Angelman syndrome
1010 mouse model. JCI Insight 6.

1011 Ostrowski LM, Spencer ER, Bird LM, Thibert R, Komorowski RW, Kramer MA, Chu CJ (2021)
1012 Delta power robustly predicts cognitive function in Angelman syndrome. Ann Clin Transl
1013 Neurol.

1014 Rotaru DC, Mientjes EJ, Elgersma Y (2020) Angelman Syndrome: From Mouse Models to
1015 Therapy. Neuroscience.

1016 Rotaru DC, van Woerden GM, Wallaard I, Elgersma Y (2018) Adult Ube3a Gene Reinstatement
1017 Restores the Electrophysiological Deficits of Prefrontal Cortex Layer 5 Neurons in a Mouse
1018 Model of Angelman Syndrome. Journal of Neuroscience 38:8011–8030.

1019 Rougeulle C, Glatt H, Lalande M (1997) The Angelman syndrome candidate gene, UBE3A/E6-
1020 AP, is imprinted in brain. Nat Genet 17:14–15.

1021 Schmid RS, Deng X, Panikker P, Msackyi M, Breton C, Wilson JM (2021) CRISPR/Cas9
1022 directed to the Ube3a antisense transcript improves Angelman syndrome phenotype in mice.
1023 J Clin Invest 131.

1024 Shi S-Q, Mahoney CE, Houdek P, Zhao W, Anderson MP, Zhuo X, Beaudet A, Sumova A,
1025 Scammell TE, Johnson CH (2022) Circadian Rhythms and Sleep Are Dependent Upon
1026 Expression Levels of Key Ubiquitin Ligase Ube3a. Frontiers in Behavioral Neuroscience
1027 16:837523.

1028 Sidorov MS, Deck GM, Dolatshahi M, Thibert RL, Bird LM, Chu CJ, Philpot BD (2017) Delta
1029 rhythmicity is a reliable EEG biomarker in Angelman syndrome: a parallel mouse and
1030 human analysis. J Neurodev Disord 9:17–14.

1031 Silva-Santos S, van Woerden GM, Bruinsma CF, Mientjes E, Jolfaei MA, Distel B, Kushner SA,
1032 Elgersma Y (2015) Ube3a reinstatement identifies distinct developmental windows in a
1033 murine Angelman syndrome model. J Clin Invest 125:2069–2076.

1034 Sonzogni M, Zhai P, Mientjes EJ, van Woerden GM, Elgersma Y (2020) Assessing the
1035 requirements of prenatal UBE3A expression for rescue of behavioral phenotypes in a mouse
1036 model for Angelman syndrome. Mol Autism 11:70–12.

1037 Spruyt K, Braam W, Curfs LM (2018) Sleep in Angelman syndrome: A review of evidence.
1038 Sleep Med Rev 37:69–84.

1039 Swayze EE, Siwkowski AM, Wancewicz EV, Migawa MT, Wyrzykiewicz TK, Hung G, Monia
1040 BP, Bennett CF (2007) Antisense oligonucleotides containing locked nucleic acid improve
1041 potency but cause significant hepatotoxicity in animals. Nucleic Acids Res 35:687–700.

1042 Willgoss T, Cassater D, Connor S, Krishnan ML, Miller MT, Dias-Barbosa C, Phillips D,
1043 McCormack J, Bird LM, Burdine RD, Claridge S, Bichell TJ (2021) Measuring What
1044 Matters to Individuals with Angelman Syndrome and Their Families: Development of a
1045 Patient-Centered Disease Concept Model. Child Psychiatry Hum Dev 52:654–668.

1046 Williams CA, Beaudet AL, Clayton-Smith J, Knoll JH, Kyllerman M, Laan LA, Magenis RE,
1047 Moncla A, Schinzel AA, Summers JA, Wagstaff J (2006) Angelman syndrome 2005:
1048 updated consensus for diagnostic criteria. In, pp 413–418. John Wiley & Sons, Ltd.

1049 Wolter JM, Mao H, Fragola G, Simon JM, Krantz JL, Bazick HO, Oztemiz B, Stein JL, Zylka
1050 MJ (2020) Cas9 gene therapy for Angelman syndrome traps Ube3a-ATS long non-coding
1051 RNA. Nature 587:281–284.

1052 Yang X (2020) Towards an understanding of Angelman syndrome in mice studies. J Neurosci
1053 Res 98:1162–1173.

1054 Zeiss CJ (2021) Comparative Milestones in Rodent and Human Postnatal Central Nervous
1055 System Development. Toxicol Pathol 49:1368–1373.

1056